4. Experimental Results

4.1 Preliminary sensor designs

The results of Equations 26 and 27 suggest the development of two designs for rheological instruments based on optical fiber strain gages. One would be intended for measurements of the complex modulus G^* of viscoelastic fluids, through the equations for G' and G''. Since measurements of the complex modulus are sensitive to the proximity of nearby surfaces, this design would incorporate fixed boundaries to eliminate any variation in this parameter. One design contemplated for this application is illustrated in Figure 4-1. The kernel of the assembly is a planar PZT actuator with a fiber optic strain gage bonded to one surface of the actuator, as detailed in Figure 3.7. To provide fixed boundaries, the sensor will be installed in a housing made of micromachined silicon. Fine gauge wires will be attached to the actuator electrodes for electrical excitation, or alternately, metallic coatings on the optical fiber could be substituted for the wires. Figure 4-2 reveals the details of the silicon components. Two separate pieces will be combined to form one side of the housing, and then two identical sides will clamp on the actuator to complete the assembly.

A second, simplified, more compact sensor is envisioned specifically for monitoring the degree of cure of thermoset resins during composite manufacturing. According to ASTM Standard D4473-90, *Standard Practice for Measuring the Cure Behavior of Thermosetting Resins Using Dynamic Mechanical Procedures*, the gel point of a composite prepreg

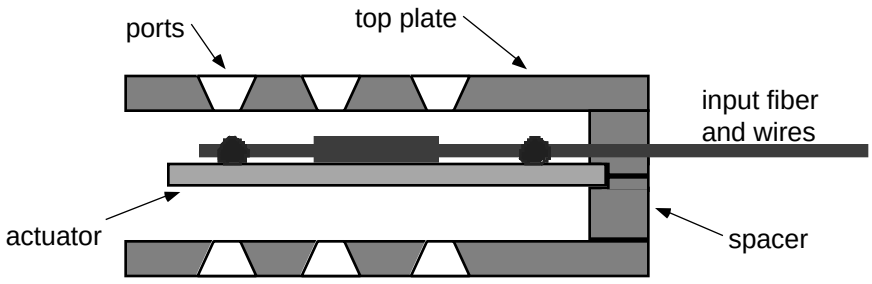

Figure 4-1. Cross-section of micromachined sensor housing.

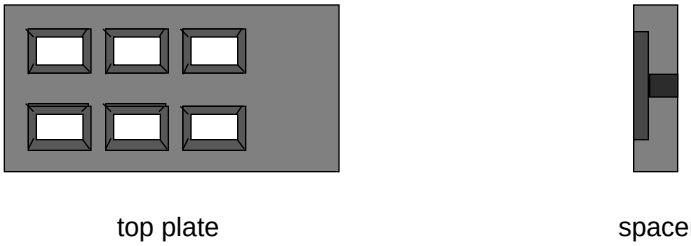

Figure 4-2. Top views of housing top plate (left) and spacer (right).

system may be determined as that point in time at which the elastic modulus levels at some asymptotic value following an increase, and after a local maximum in loss tangent (tan delta) is observed.[39] From Equation 31, the loss tangent can in principle be derived from the phase difference between the actuator excitation and the strain gage output, if the terms involving the mechanical impedance of the silicone elastomer can be neglected. In practice, however, the phase difference measured is that between the voltage applied to the high voltage amplifier connected to the actuator, and the voltage output by the optoelectronic system which processes the output of the fiber optic strain gage. Both the amplifier and the optoelectronic system introduce constant phase delays which are not accounted for by Equation 31. Since the electronic phase delays are constant, the relative change in phase difference can still be used to determine the occurrence of a maximum in the loss tangent during cure. Also, as indicated by Equation 33, the strain amplitude output by the sensor may be used to track changes in the absolute shear modulus, for those cases in which the change in boundary separation is much less than the expected change in modulus, which is the case for the cure of composite prepreg material.

---

[39] Standard D 4473-90, "Standard Practice for Measuring the Cure Behavior of Thermosetting Resins Using Dynamic Mechanical Procedure", Annual Book of ASTM Standards, Vol. 08.03, American Society for Testing and Materials (ASTM), Philadelphia, PA .

4.2 Test of sensitivity to boundary conditions

Equations 26 and 27 of the analytical model suggest that the sensor outputs for a test resin with a fixed complex modulus will be a function of the separation of the actuator from adjacent boundaries. Specifically, for measurements of a viscoelastic fluid with a constant modulus, the measured strain amplitude ε_0 should increase linearly as the separation c increases. According to Equation 31, the phase difference φ should be independent of the separation for cases in which terms involving the silicone rubber immitances may be ignored (for instance, when $c << 2A$). In order to test these predictions and validate the model, an experiment was undertaken to investigate empirically the dependence of the sensor output on boundary effects. An apparatus was assembled to permit the separation of the actuator surfaces from adjacent boundaries to be varied. Using aluminum materials, a box was constructed so that it could easily be disassembled for cleaning after tests. As shown in Figure 4-3, an L-shaped bracket was fitted with tracks and a micrometer so that the position of the box could be varied laterally by a known amount. A clamp was mounted to the L-shaped bracket to hold the sensor in the box, on the end of a rod at a fixed distance from the side of the bracket. By adjusting the micrometer, the distance separating the sensor from the closest interior wall of the box could be controlled. Next, an aluminum cube was machined to fit as a piston inside the box, and a second micrometer was mounted in one wall of the box to control the placement of the piston. Adjusting this second micrometer moved the position of the piston in the box, and hence changed the separation of the piston from the sensor. By careful adjustment of the two micrometers, the separation of the two broad actuator surfaces from the closest two interior walls of the box could be varied. The inner dimensions of the box were 12.7 mm wide, 25.4 mm deep, and 12.7 mm long (maximum).

To fabricate a prototype sensor, a 38 mm x 64 mm x 0.19 mm (1.5 in x 2.5 in x 0.0075 in) PZT-5A plate was diced into 5 mm x 15 mm (0.2 in x 0.6 in) coupons. The plate had been electroded using an electroless nickel plating process by the manufacturer, and was poled across the thickness of the plate. Two 34 AWG wires with polyurethane insulation were attached to the electrodes of one of the small coupons using a metal-filled conductive epoxy. Next, a fiber optic strain gage of the EFPI configuration was constructed by cleaving and inserting one end of an 830 nm single mode, 125 μm diameter optical fiber into a 130 μm inner diameter, one centimeter long fused silica capillary tube, and fixing the fiber in place with a high temperature epoxy where the fiber entered the capillary tube. A

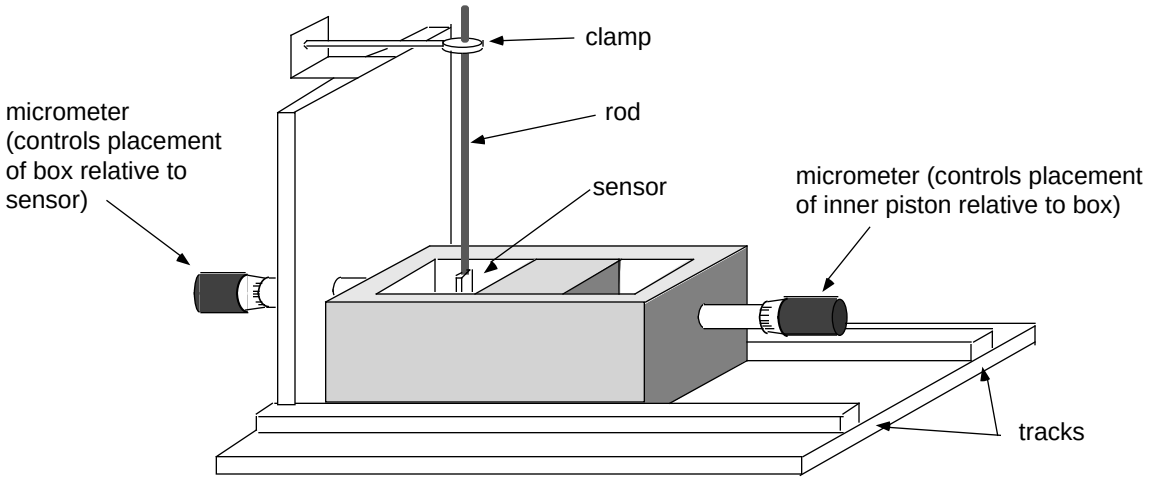

Figure 4-3. Apparatus used to test dependence of sensor output on boundary conditions.

reflector fiber was fashioned by cleaving one end of a one centimeter long, 125 μm diameter multimode optical fiber, and inserting it into the remaining open end of the capillary tube. The reflector fiber was temporarily attached to a micropositioner, and the separation of the two fiber ends was adjusted to approximately 50 μm while monitoring the separation through the use of an absolute fiber sensor system. When the correct gap was achieved, a silicone rubber adhesive was applied to the end of the capillary tube where the reflector fiber exited the tube. The fiber optic strain gage was then attached to one surface of the PZT actuator by using two spots of high temperature epoxy to bond the optical fibers to the actuator. The epoxy, which was cured at 200°C for one-half hour, was measured to have a glass transition temperature of 140°C by differential scanning calorimetry. One epoxy spot was applied to the single mode input fiber, and the other to the multimode reflector fiber, as shown in Figure 3.1. In this way, any elongation of the actuator will be transferred to the EFPI strain gage, resulting in a change in the separation of the two fiber ends in the capillary tube. By monitoring the optical power and spectrum reflected by the sensor, the gap distance, and hence that actuator elongation, can be determined through the methods described in Section 3.1.

The end of the actuator/strain gage assembly was attached by epoxy to a 1.6 mm (1/16 in) diameter wooden rod, taking care to insure that the attachment would not constrain the vibration of the actuator. The free end of the rod was mounted onto a clamp, as shown in Figure 4-4, so that the sensor assembly was held inside the aluminum box. The box was

then filled with honey, obtained at a grocery store. Honey was chosen as a viscoelastic test specimen, since no calibrated standards for viscoelastic materials current exist, and honey is inexpensive, non-toxic, and easily cleaned. The real and imaginary components of the complex modulus of the honey used were measured using a Rheometrics RDS 800 Dynamic Spectrometer over the frequency range of interest, and are reproduced in Figure 4-5.

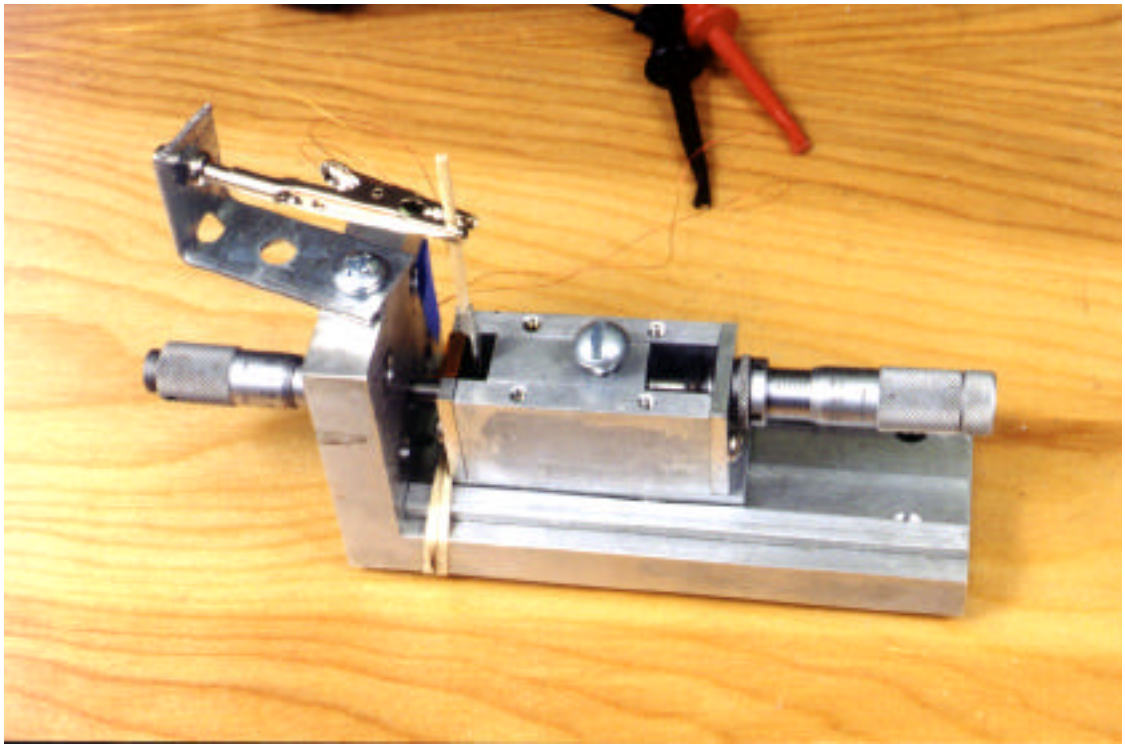

Figure 4-4. Photograph of apparatus for testing boundary dependence of sensor output.

A Stanford Research SR810 digital lock-in amplifier was used to generate the sinusoidal steady state ac voltage used to drive the actuator. The 5V "sine out" signal from the lock-in amplifier's internal oscillator was boosted to 300V peak-to-peak by an ACX, Inc. EL1224 high voltage amplifier designed to drive capacitive loads such as piezoelectric devices, as shown in Figure 4-6. The optical signal output by the fiber optic strain gage was converted to a voltage proportional to the measured strain by an absolute fiber sensor system, as described in Section 3.1. The voltage output by the sensor system had been previously

calibrated so that the sensor strain amplitude could be determined from the voltage. The electrical signal out of the absolute fiber sensor system was input to the lock-in amplifier, which measured the magnitude of the strain signal and the phase delay between the internal oscillator of the lock-in amplifier and the strain gage signal output by the absolute fiber sensor system. As pointed out previously, this phase delay will include not only contributions due to the viscoelastic damping of the test specimen, but also delays due to the high voltage amplifier and the optoelectronic system. The use of a lock-in amplifier, which is a narrow-bandpass voltmeter that employs synchronous (phase-sensitive) detection to lock onto a signal, permits accurate measurements of strain amplitude and the phase delay even in the presence of noise levels exceeding the strain signal amplitude. The digital lock-in amplifier employed in this study was optimized for measurements of signals at sub-Hertz frequencies.

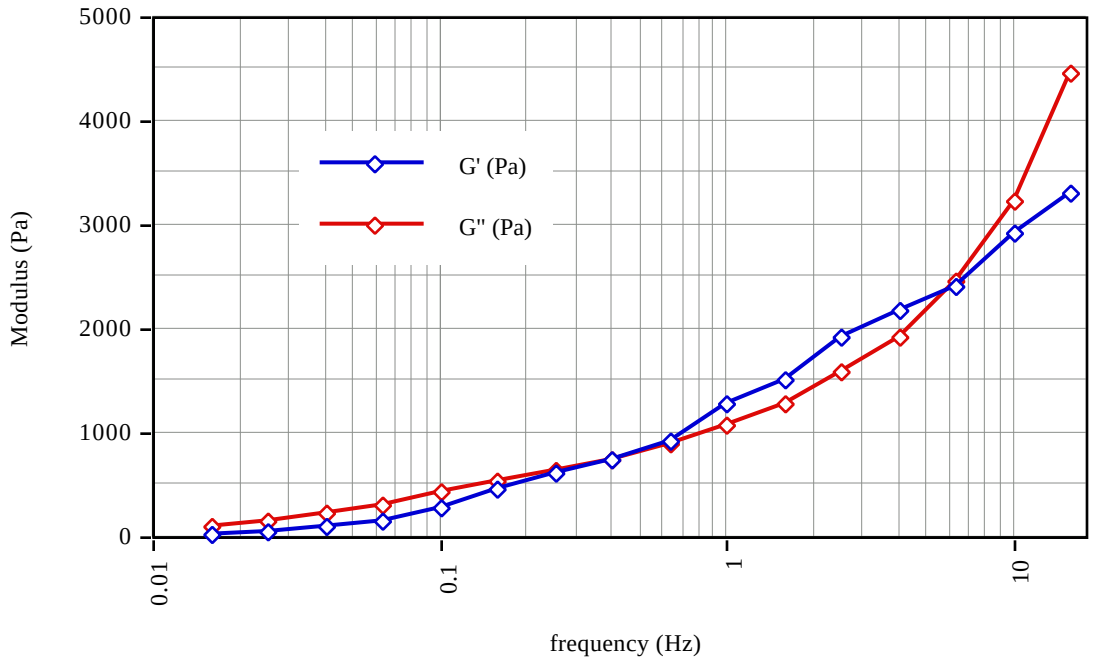

Figure 4-5. Rheological characterization of honey used in boundary experiments, as obtained using a Rheometrics RDS 800 Dynamic Spectrometer.

The phase and magnitude data output by the lock-in amplifier was acquired by a laptop computer over a GPIB interface, using a program written in National Instruments LabVIEW to automate the data collection (Appendix A). The computer was programmed to acquire data at five different frequencies, from 0.5 Hz to 10.0 Hz, after each adjustment of the

boundary separation. In addition, the temperature of the assembly was monitored by mounting a Type J thermocouple onto the actuator, and capturing the thermally generated voltage through a National Instruments DAQ700 digital/analog (D/A) card in the computer. The data acquisition was repeated five times in order that the standard deviation of the data could be determined.

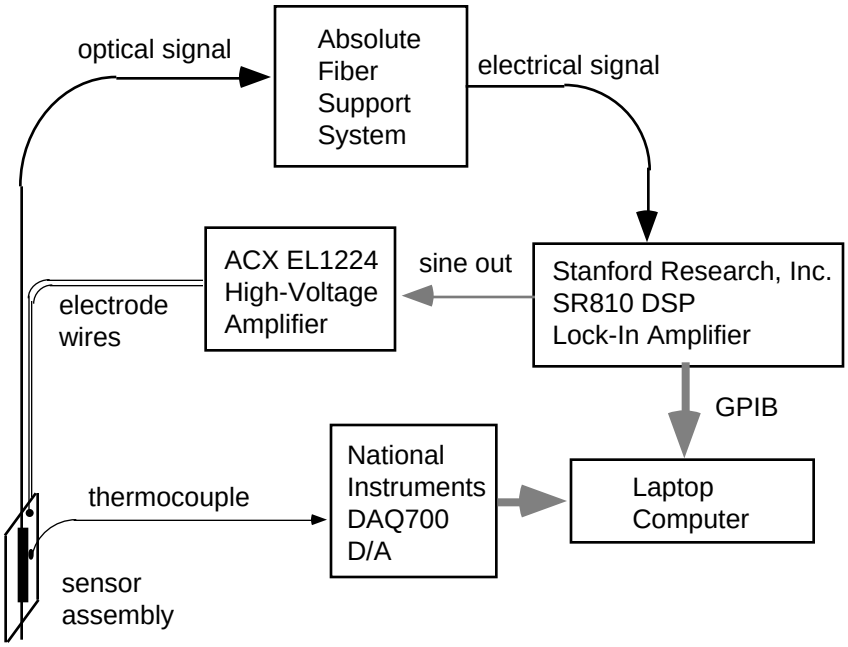

Figure 4-6. Instrument interconnection for testing of prototype sensors.

The test results are plotted in Figure 4-7 and Figure 4-8, where the data plotted represent the mean of five measurements at each separation. The two micrometers were adjusted so that the separation of the box walls from the actuators was equal on both sides of the actuator. Due to the presence of the fiber strain gage on one side of the actuator, the smallest separation achievable was approximately one millimeter. Since the maximum travel of the piston in the box was about 12 mm, the maximum separation was 6 mm.

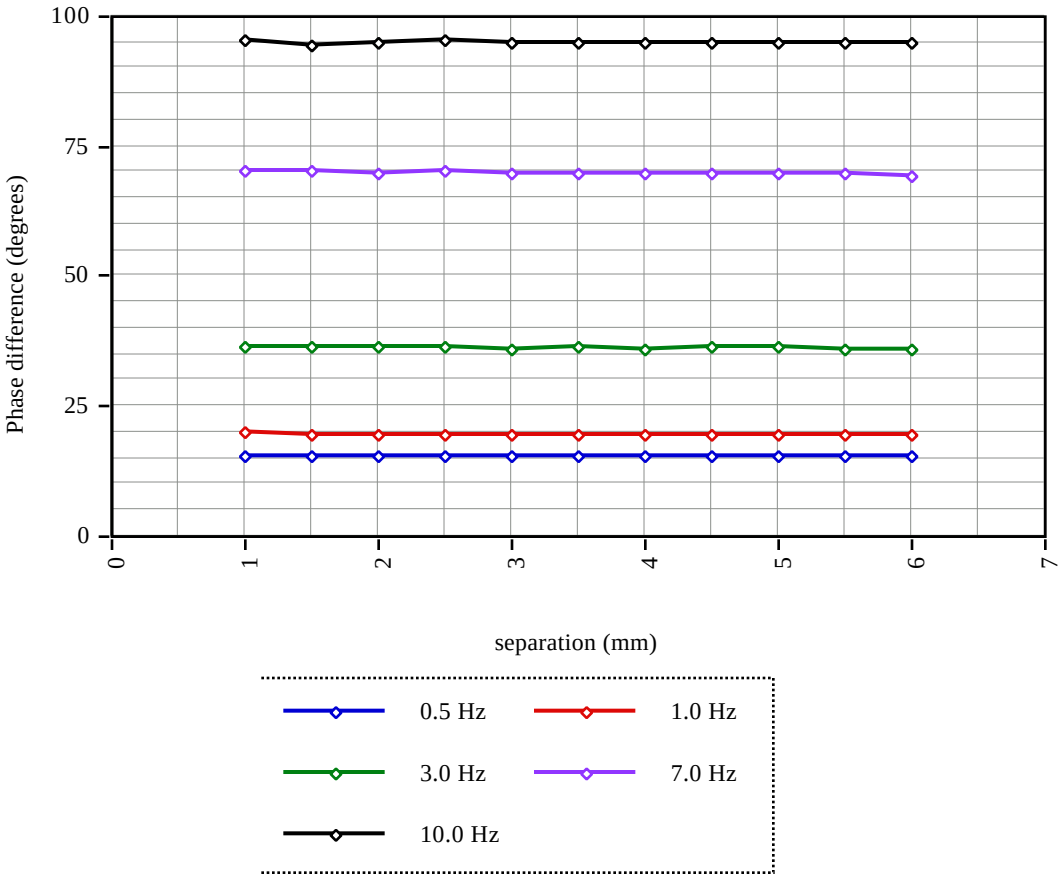

Figure 4-7. Plot of phase delay for varying separation of actuator and boundaries, for five frequencies.

Since the standard deviations for the measurements shown in Figure 4-7 and Figure 4-8 are below the resolution of the plots, Figure 4-9 reproduces the test results for phase difference and strain amplitude for 0.5 Hz excitation only. The standard deviations for the five measurements at each separation are displayed as error bars in the figure.

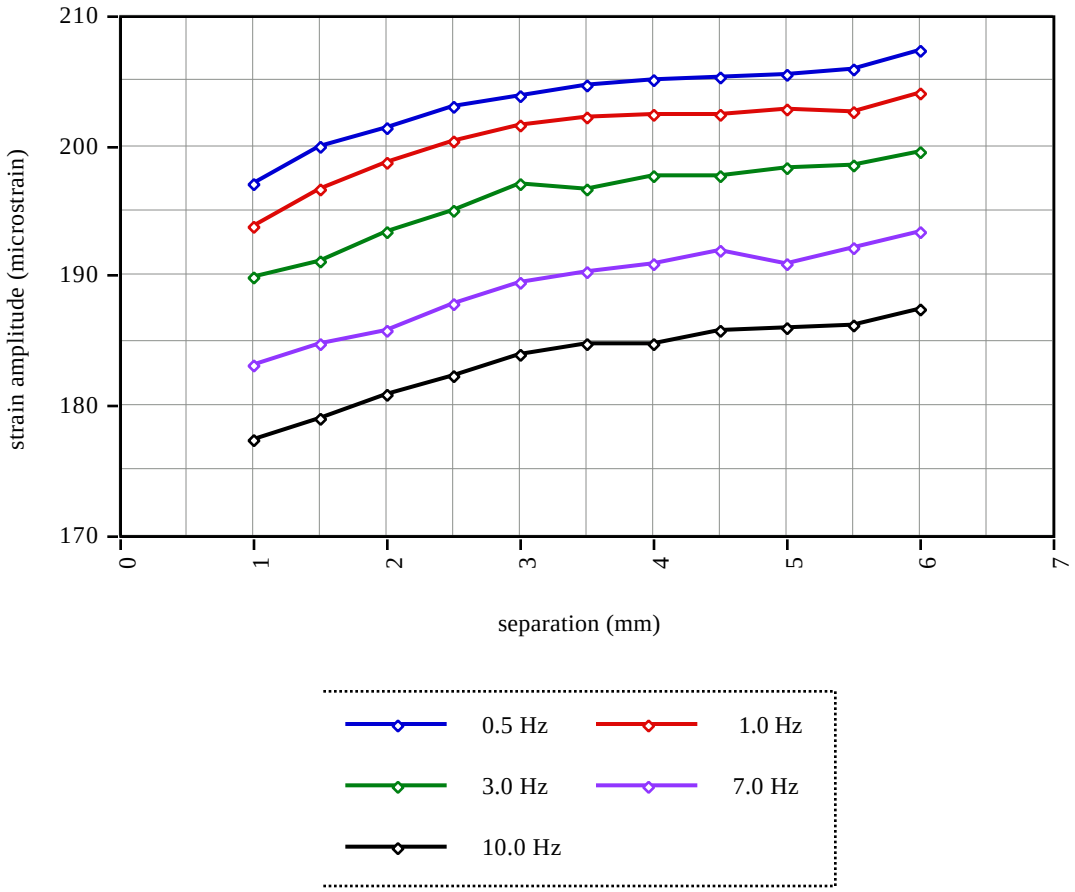

Figure 4-8. Plot of strain amplitude for varying separation of actuator and boundaries, for five frequencies.

While the phase difference between excitation and response as shown in Figure 4-7 is independent of the actuator-boundary separation, it is clearly dependent on the excitation frequency. This behavior is a consequence of the existence of frequency ω in the terms including the silicone rubber immittances in Equation 32. The results of Figure 4-7 may be used to derive estimates for the silicone rubber immitances F_s and E_s.

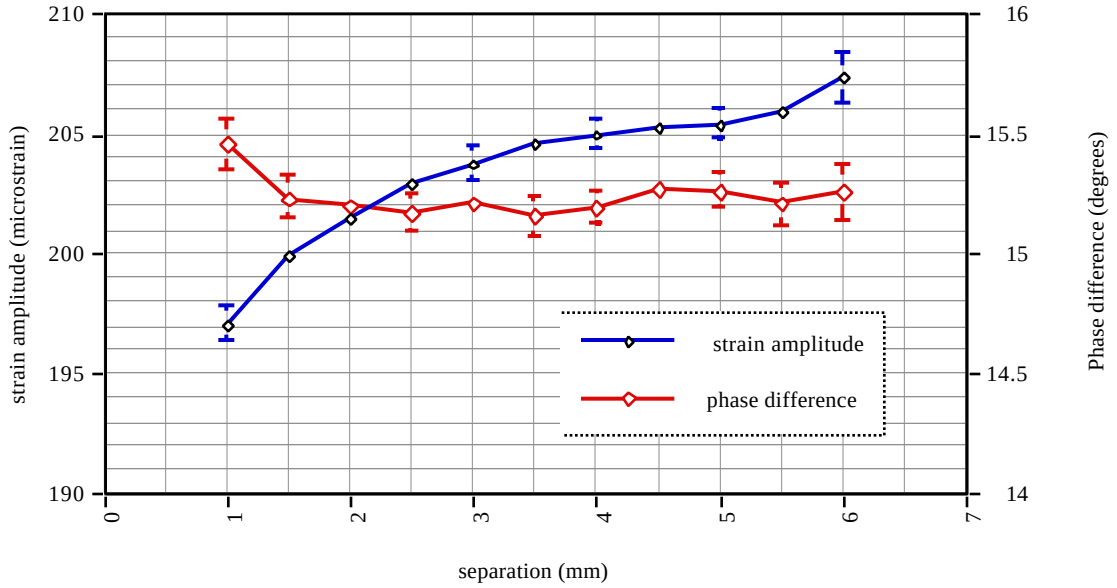

Figure 4-9. Plot of strain amplitude and phase difference at 0.5 Hz excitation, showing standard deviation as error bars for each measurement.

Since the shear moduli *G'* and *G"* are known for the test specimen honey at a particular frequency ω_1, then Equation 31 may be written as

$$\tan\varphi(\omega_1) = \frac{G''(\omega_1) + c\omega_1\frac{F_s}{2A}}{G'(\omega_1) + c\left(\frac{E_s}{2A} - \omega_1^2\frac{I_s}{2A}\right)}. \qquad (62)$$

By substituting the measured values for tan φ for each separation value *c* used in the measurement, which were plotted in Figure 4-7, a set of overdetermined linear equations results. For example, at the excitation frequency of 0.5 Hz, G'= G"= 800 Pa for honey, and the Equation 62 takes the form of

$$\frac{800 + cx}{800 + cy} = \tan\varphi \quad 0.27, \qquad (63)$$

where $x = (\omega/2A)F_s$ and $y = (1/2A)E_s$, and where the term involving the inertance I_s is much smaller than the elastance term. Appendix B lists the eleven equations that result from

varying the separation *c* from 1 mm to 6 mm in 0.5 mm steps. A program written as a MATLAB script to determine the best fit for *x* and *y* is also listed in Appendix B. The results indicate that

$$x = 1.245 \text{ x } 10^4 \tag{64}$$

and

$$y = 4.65 \text{ x } 10^4, \tag{65}$$

from which

$$F_s = 594.4 \text{ Pa·m·s}, \tag{66}$$

and

$$E_s = 6978 \text{ Pa·m}. \tag{67}$$

These results are approximately an order of magnitude higher than the values predicted in Section 3.3, in which measurements of the sensor geometry and silicone rubber rheology led to calculations yielding Es = 234 Pa·m and Fs=390 Pa·m·s. This discrepancy is likely due to inaccuracies in measurements of the geometrical factors A_s and L_s.

To examine the role of the immittance parameters, the values for F_s and E_s determined above were substituted into Equation 31, and the phase difference φ was calculated for separations ranging from 1.0 to 6.0 mm. The results are plotted for five frequencies in Figure 4-10. As the results show, the frequency dependence and the ordering of the data by frequency seen in the experimental data of Figure 4-7 are reproduced, although the numerical values of the phase angles from the experimental data are not strictly reproduced.

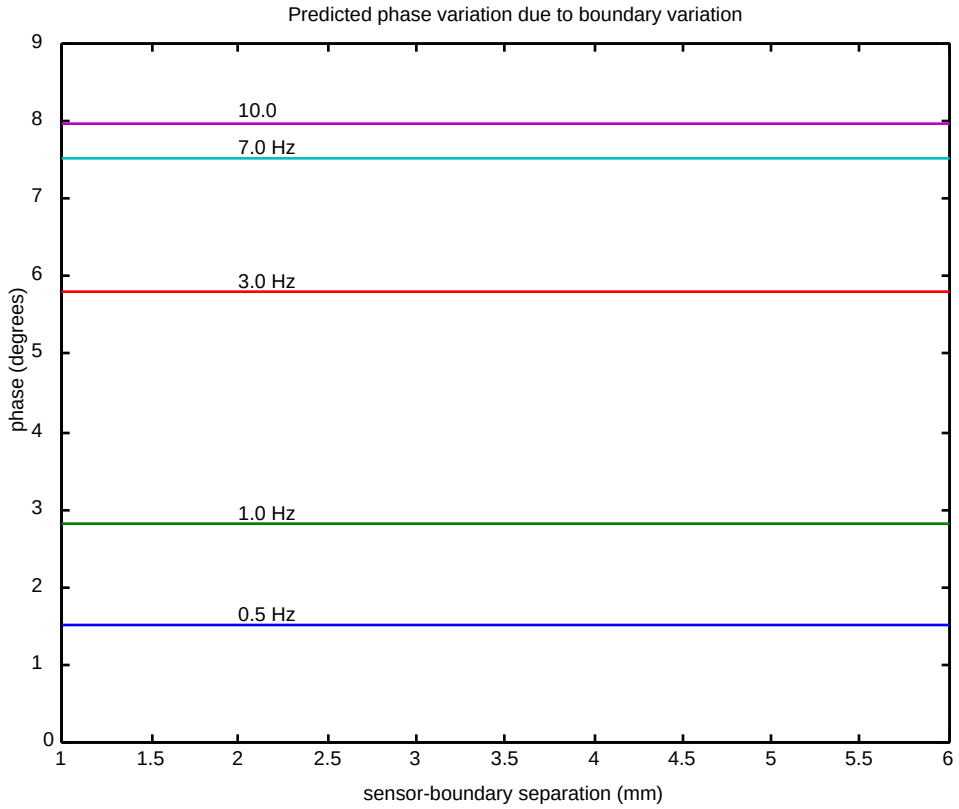

Figure 4-10. Plot of predicted phase difference as a function of frequency, using values for F_s and E_s in Equations 66 and 67.

To further investigate the sensor response over an extended range of boundary separation, a second test fixture was made by taking a plastic box with inner dimensions of 64 mm wide x 64 mm deep x 145 mm long, and installing a plastic sheet inside the box with silicone rubber to form a new inner wall, so that the resulting dimensions of the box were 64 mm x 64 mm x 44 mm. Additional plastic sheets were cut to place inside the box as shims to reduce the length of the inside cavity. In this way, the prototype sensor could be placed inside the box, and the actuator-boundary separation could be varied by removing or adding plastic shims from the inside of the box. A total range of separations from 4 mm to 13.8 mm was possible in this manner.

To obtain data with extended separations, the prototype sensor was placed inside the box, held in place by a wooden rod, which was clamped on one end (Figure 4-11). Nineteen shims were added to the cavity, which reduced the separation of the actuator from the walls to approximately 4 mm on both sides. Honey was added, and the first data point, consisting of a measurement of phase and amplitude, was taken. After each data point was obtained, one shim was removed, more honey was added to maintain the liquid level, and another data point was obtained. After each shim was removed, the position of the sensor assembly was adjusted by hand, until it was judged by visual inspection to be approximately centered in the cavity. This proceeded until eleven shims had been removed.

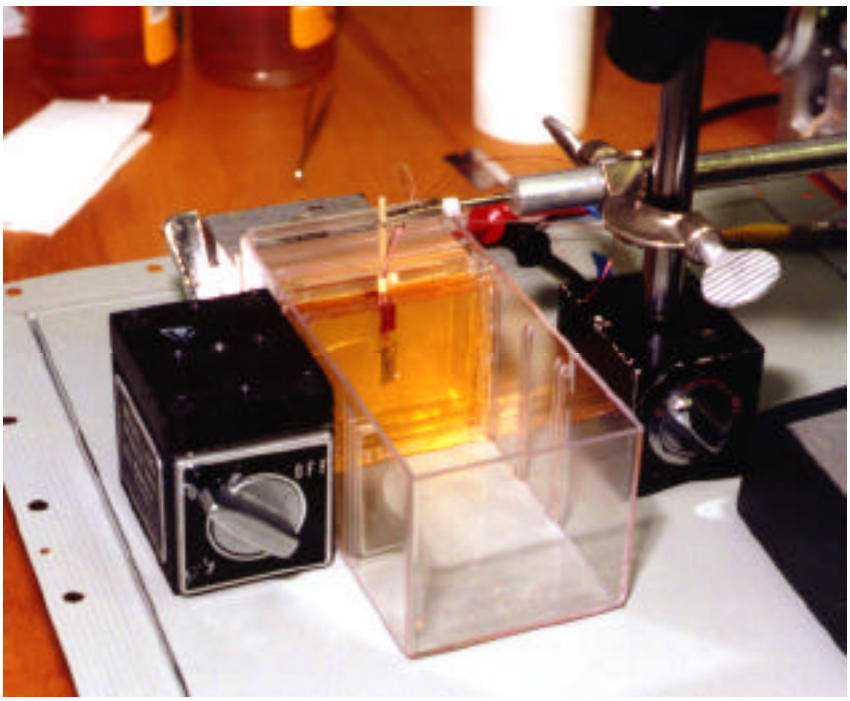

Figure 4-11. Photograph of test fixture for tests of extended boundary separations.

The measurement of amplitude and phase in the original aluminum box with micrometer control was repeated, and then the sensor assembly was transferred to the plastic box for measurements over the extended separation range. During transfer of the sensor, the actuator was accidentally fractured, so that a new sensor assembly was used for the test in the plastic box. When the strain amplitude signal data from the sensor in the box is added to the corresponding data obtained in the aluminum box, the plot in Figure 4-12 results.

The blue curve corresponds to the data taken in the aluminum box, and the red curve corresponds to the data for extended separations taken in the plastic box. The maximum amplitudes for the two sensors differ, presumably due to differences in attaching the sensor to the holding fixture, so that the magnitudes of the two curves were adjusted in the plot in Figure 4-12 to show the trend in the data.

The results of the experiment indicate that the strain amplitude ε_0 varies approximately linearly with the boundary separation for small gaps, but then approaches an asymptotic limit for large separations. This limit is expected, since a physical limit to the maximum strain developed by the PZT actuator exists. This limit is imposed by either the product of the applied electric field multiplied by the piezoelectric coefficient, or the maximum rated voltage preceding dielectric breakdown (typically the breakdown occurs in the medium surrounding the actuator), or the maximum rated stress.

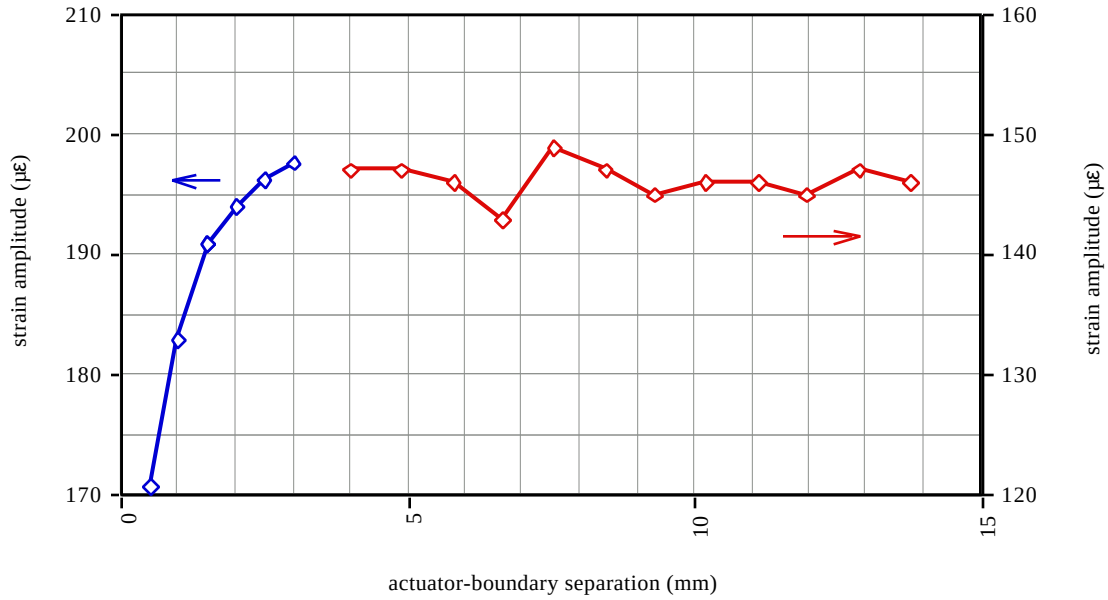

Figure 4-12. Plot of the strain amplitude output by sensor for extended boundary separations. The offset between the sensor used for short separation (in blue) and the sensor used for long separations (in red) was adjusted to make the trend appear continuous.

In this case, the maximum strain developed by the actuator is limited by the applied electric field:

$$\varepsilon_{max} = d_{31}\frac{V_0}{t} = \left(-2.0x10^{-10}\frac{m}{V}\right)\left(\frac{150\ V}{1.9x10^{-4}}\right) = -157x10^{-6}, \tag{68}$$

where V_0 is the amplitude of the applied voltage, and t is the thickness of the actuator. Here the value for the piezoelectric coefficient used was determined by applying a dc voltage to the actuator in air, and measuring the resulting strain using the attached EFPI fiber optic strain gage. The magnitude for the predicted maximum strain amplitude agrees well with that measured during the test, as shown in Figure 4-12.

4.3 Tests of prototype sensor in neat resin.

The prototype sensor illustrated in Figure 3.1 was tested in two commercially available neat (no reinforcing fibers) epoxies: Devcon Two-Ton Epoxy and a high performance epoxy formulated especially for resin transfer molding (RTM) applications. The RTM resin, which cannot be identified due to clearance concerns by the research sponsor, will be denoted as RTM-1 in the research that follows. The Devcon resin, a two-part room temperature curing resin, was chosen for its rapid cure and ease of use. It employs a diglycidyl ether of bisphenol A resin with an aminoethylpiperazine hardening agent. The RTM-1 epoxy , a one-part low viscosity resin with a premixed latent curing agent, was chosen as a representative high performance resin commonly used by the aerospace industry. The exact formulation is proprietary, but it is based on a diglycidyl ether of fluorine bisphenol. The amine-based curing agent melts at 145°C. The tests described in this section were intended to determine if the sensor outputs varied in a manner consistent with the predictions of the analytical model.

4.3.1 Characterization of test resins

4.3.1.1 Devcon Two-Ton Epoxy

Differential scanning calorimetry (DSC), viscometry, and dynamic mechanical analysis (DMA) tests were performed on samples of curing Two-Ton epoxy and RTM-1 epoxy, in order to obtain insights into the mechanical behavior of the resins during cure. For the Two-Ton epoxy, an isothermal DSC scan of the resin indicated that the peak reaction exotherm occurred at about the time that the DSC pan containing the freshly mixed resin was placed in the instrument (Figure 4-13). Mixing of the resin and hardener, placement of a mixed sample into a DSC pan, crimping of the pan, and placement of the pan into the

DSC chamber took approximately 14 minutes. This loss of data from the initial stages of cure makes the determination of degree of cure through DSC measurements difficult.

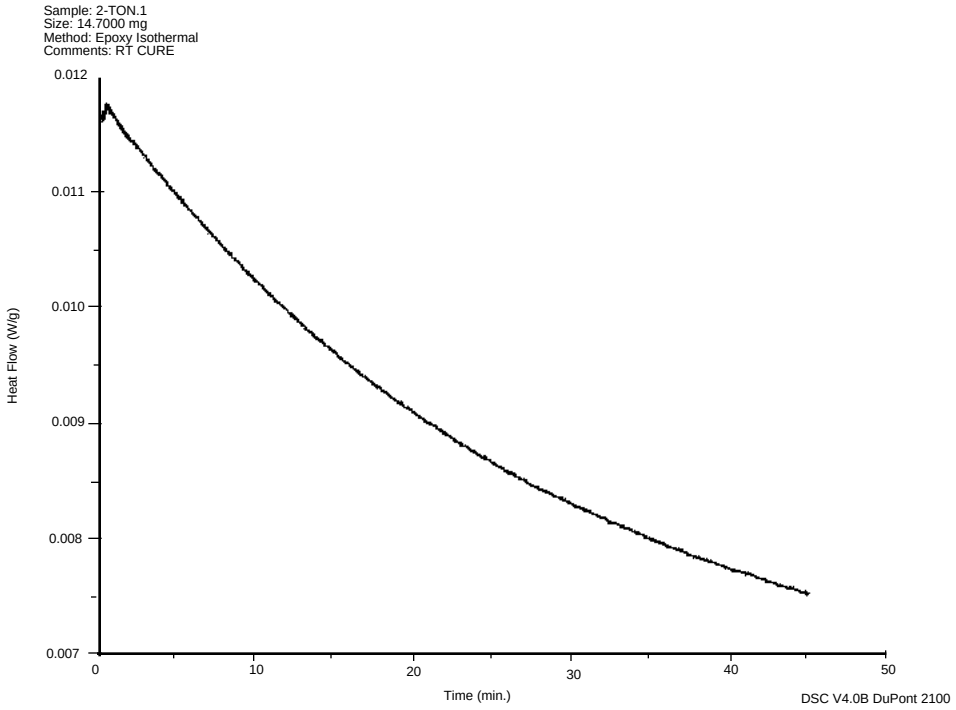

Figure 4-13. Differential scanning calorimeter output for curing Devcon Two Ton epoxy. Fourteen minutes elapsed from the time the resin and hardener were mixed until the time the DSC measurement was started at the time 0 min. indicated on the plot.

Measurements of the steady shear viscosity of the Two-Ton epoxy during cure using a Brookfield viscometer with a rotating rod in a cylinder shows a sharp increase in viscosity as the cure proceeded (Figure 4-14). At 800 seconds (~ 13 minutes), the sample sheared off the surface of the oscillating rod. However, the trend in viscosity appears to be consistent with a gel point ($\eta \rightarrow \infty$) of about 20 minutes.

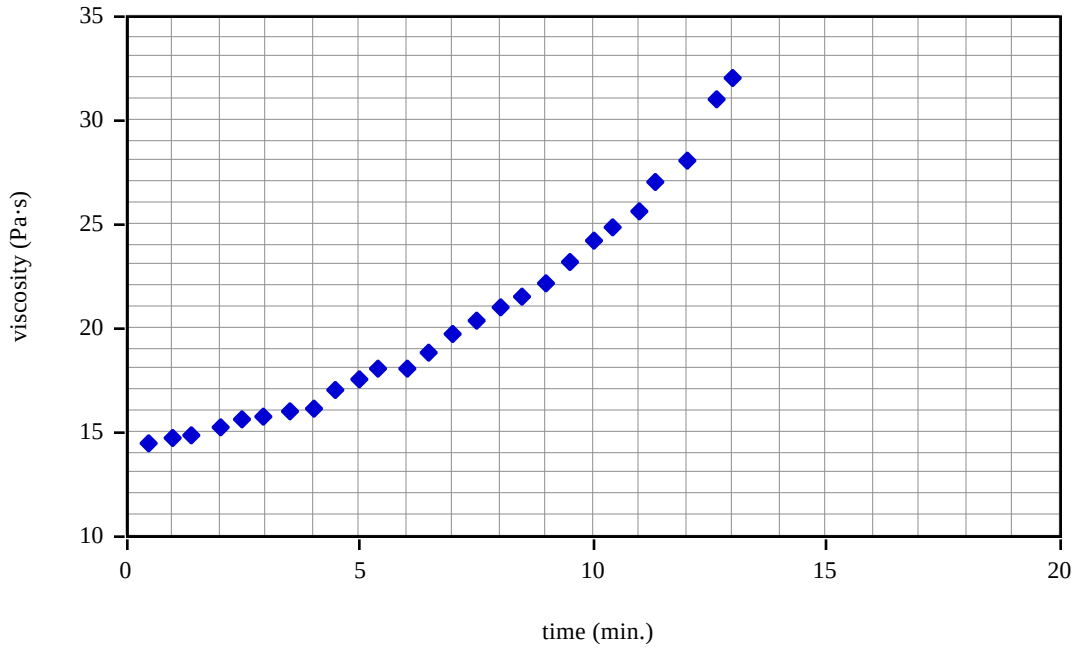

Figure 4-14. Measurement of viscosity of Devcon Two-Ton epoxy during cure.

Dynamic mechanical analysis of Devcon Two-Ton epoxy curing at room temperature was performed using a Rheometrics RDS 800 mechanical spectrometer at 0.5 Hz, 1.0 Hz, and 10 Hz with variable strain. The results for the 1 Hz test are illustrated in Figure 4-15. For times greater than 30 minutes, the sample occasionally slipped from the parallel plate fixtures, resulting in some data points for which $G'=0$. Those points have been omitted from the plot to clarify the trends. The test was concluded when adhesion between the parallel plates and the test specimen was completely lost. As the figure illustrates, the loss modulus G'' rose steadily during the test, and the storage modulus G' also increased, though at a lesser rate. The loss tangent was calculated from the data by taking the ratio G''/G', and then the loss angle δ was determined by taking the arctangent of the ratio. The result, also plotted in Figure 4-15, indicates that the trend in the loss angle is increasing over the 45 minute duration of the test. The low values for G', and the fact that G' never exceeds G'', suggests that the resin was not fully cured at the conclusion of the 48 minute test.

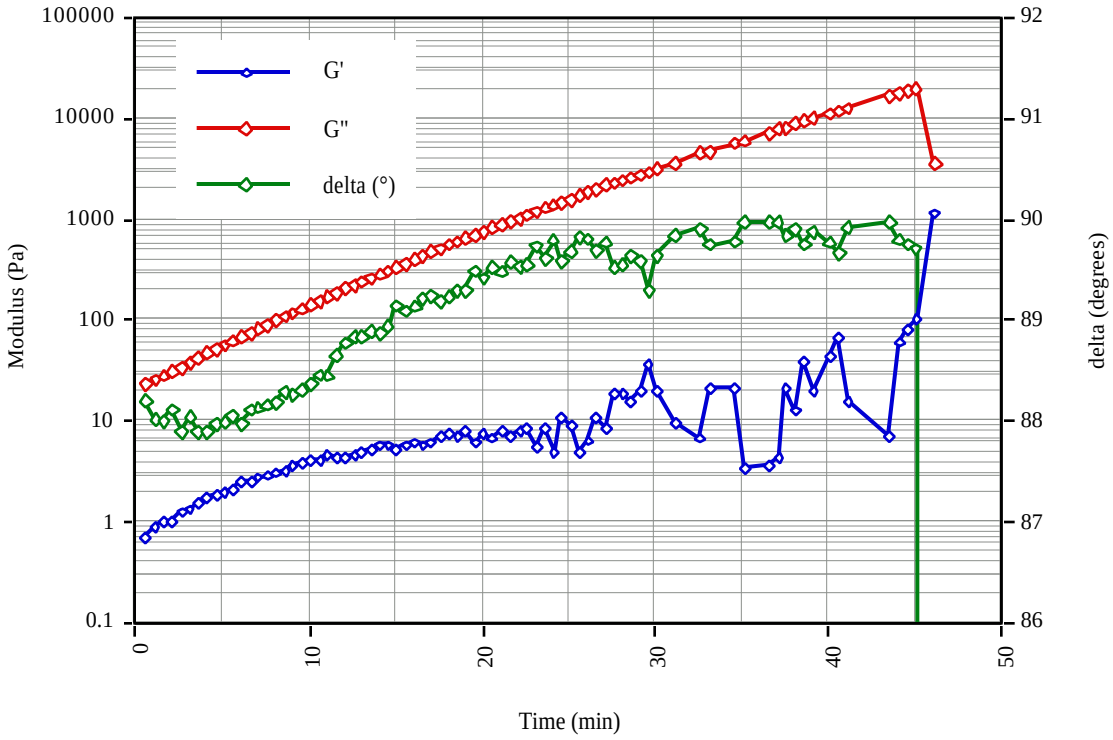

Figure 4-15. Dynamic mechanical analysis results for Devcon Two-Ton epoxy during cure at room temperature, using a Rheometrics 800 mechanical spectrometer at 1 Hz excitation with variable strain.

In order to extend the duration of the test, the DMA test was repeated with a fresh sample of Devcon Two-Ton epoxy, with the strain excitation set to 0.16 Hz (1.0 radians/s). By decreasing the excitation frequency, the strain rate is also reduced, which was expected to minimize the tendency of the sample to separate from the fixture plates. Figure 4-16 and Figure 4-17 show the results of the test. The recording of G' and G'' data was halted in the interval from 42 minutes to 50 minutes after the start of cure, so that the Rheometrics system could be used to perform a frequency scan over a range from 0.1 rad/s (0.016 Hz) to 100 rad/s (16 Hz). Since the frequency scan in Figure 4-17 showed that $G''>G'$ for the frequency range tested, it was decided that the epoxy was not fully cured, and the measurement of the storage and loss moduli were resumed at 50 minutes after the start of the test.

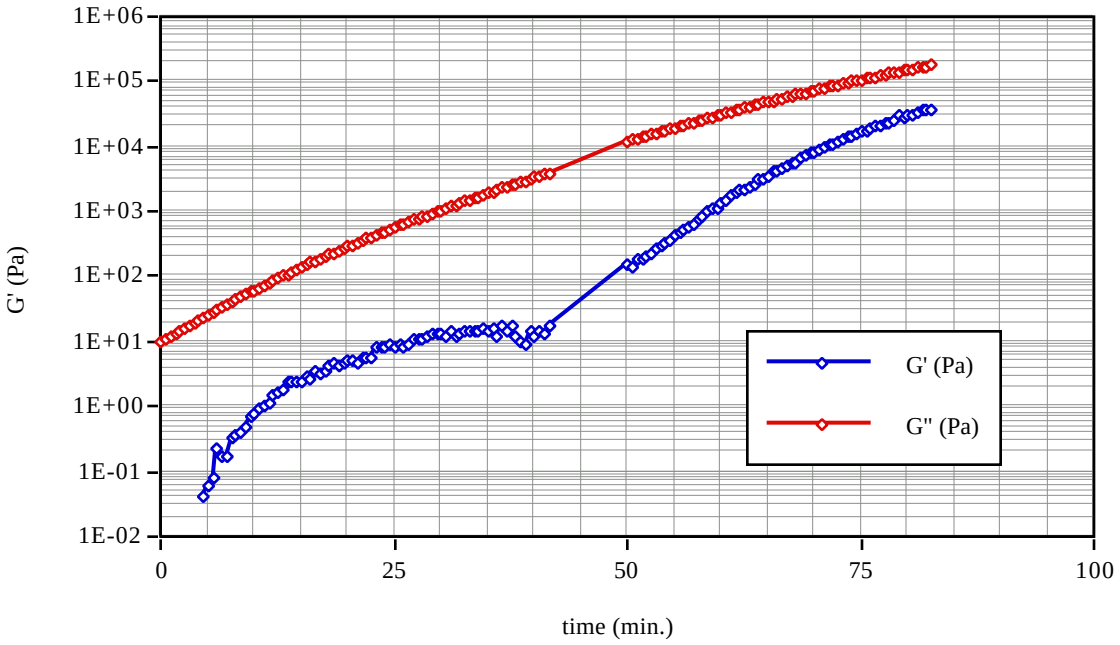

Figure 4-16. Dynamic mechanical analysis results for Devcon Two-Ton epoxy during cure at room temperature, using a Rheometrics RDS 800 mechanical spectrometer at 0.16 Hz excitation with variable strain.

Eighty-three minutes into the test, the test was stopped automatically when the loss modulus exceeded the capacity of the Rheometrics spectrometer (approximately 10^5 Pa). The trend shows the value of the storage modulus approaching that of the loss modulus, although the value of the storage modulus still remains below the loss modulus value for the test duration. This behavior is consistent with the manufacturer's instructions for use of the resin, which states that the partially cured resin can be moved two hours after mixing, and attains full strength (fully cured) in eight hours at room temperature.

The loss tangent for the second DMA test of the Two-Ton epoxy was calculated by taking the ratio of the loss modulus to the storage modulus as reported in Figure 4-16. The resulting curve, in Figure 4-18, shows that the loss tangent achieved a local maximum forty minutes into the test, indicating the occurrence of a rheological transition at that point, which appears to be associated with gelation. As pointed out in Section 2.2, epoxies cured at temperatures less than T_{gg}, the temperature at which vitrification and gelation occur

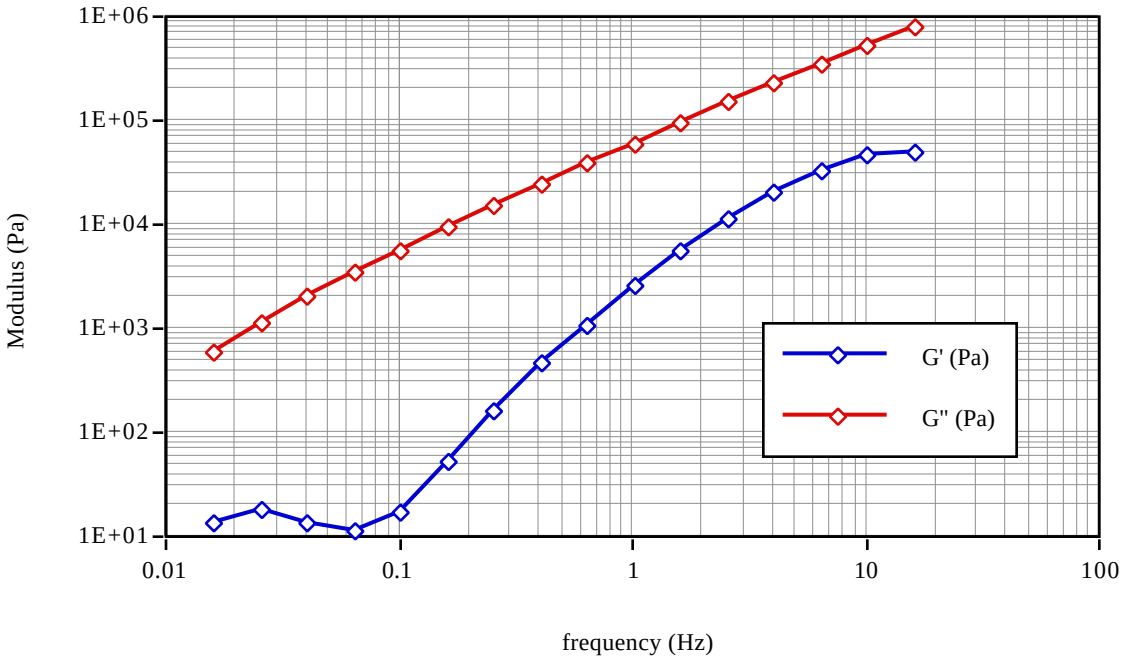

Figure 4-17. Dynamic frequency scan for Devcon Two-Ton epoxy at room temperature forty-two to fifty minutes after mixing, using a Rheometrics 800 mechanical spectrometer .

simultaneously, will vitrify due to increasing molecular weight, without gelation. Since the T_{gg} has not been characterized during this research for Two-Ton epoxy, it is conceivable that the transition indicated by the loss peak during the DMA tests could be associated with vitrification. However, the resin's manufacturer indicates that a 100 g sample will gel in fifteen minutes at 70°F (21°C), with longer gel times exhibited for smaller samples.[40] Since the DMA test employed a sample with a mass of 0.5 g, it appears reasonable to conclude that the loss peak in Figure 4-18 is associated with gelation.

The mechanical behavior of curing Two-Ton epoxy was also characterized at 25°C using a Netzsch DMA 242 dynamical mechanical analyzer operated in the dual cantilever mode using a customer sample holder. To perform the test, a carbon fiber braid approximately 18.5 mm long by 10.0 mm wide by 2.0 mm thick was impregnated with uncured freshly mixed epoxy. The braid was clamped into the DMA fixture, and a probe which contacts

[40] Devcon, Inc., Technical Support, 800-993-8266.

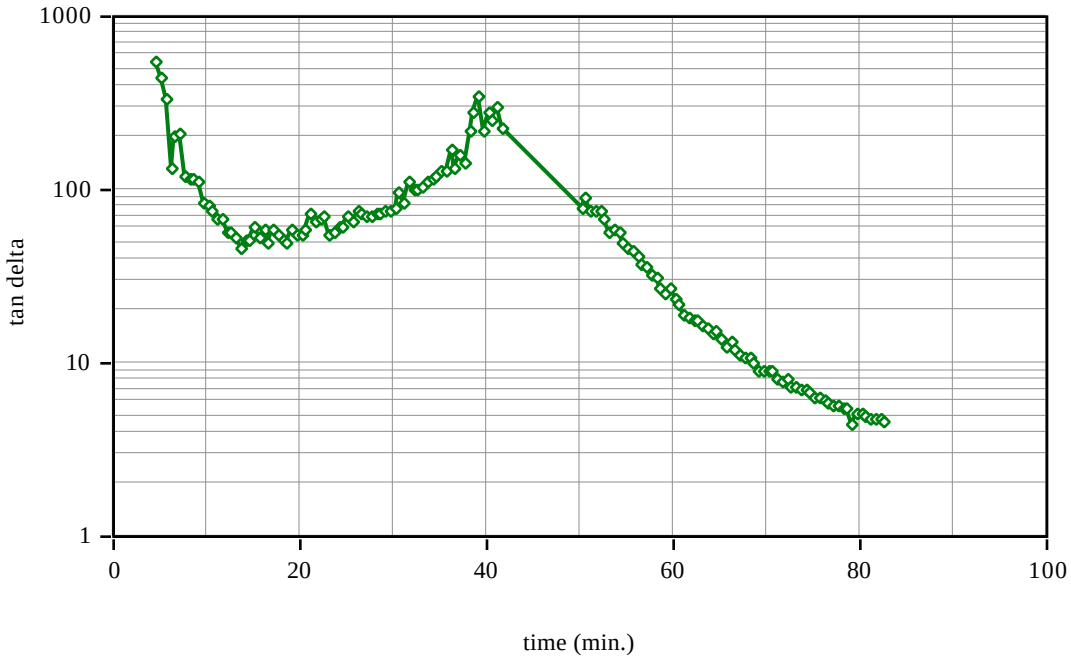

Figure 4-18. Loss tangent (tan δ) for Devcon Two-Ton epoxy curing at room temperature.

the center of the braid induces sinusoidally time-varying 3-point bending at a known amplitude and frequency. By measuring the force required to achieve the set bending amplitude, and the phase difference between the force and the displacement, the bending stiffness, which is the product of the modulus and the moment of inertia of the impregnated braid, is derived. Since the moment of inertia changes only slightly due to thickness changes in the specimen, the complex modulus and loss tangent may be determined as a function of cure time.

As the results shown in Figure 4.19 show, a peak in the loss tangent is observed approximately fifty minutes after the beginning of the test. No other peaks were detected over the period of the twelve hour test. Due to the influence of the carbon fiber braid on the measurement of modulus, values for the storage modulus E' shown in the plot are relative, and are useful only for displaying trends. From the figure, it can be concluded that the storage modulus increases by more than an order of magnitude during the cure.

4.3.1.2 RTM-1 Epoxy

The isothermal DSC scan in Figure 4-20 for RTM-1 epoxy curing at 180°C shows that the peak exotherm occurred at about 14 minutes from the application of the elevated temperature. Viscometry by the Brookfield viscometer suggests in Figure 4-21 that gel point, as measured by the viscometer, occurs at approximately 19 minutes into the cure for an isothermal temperature of 180°C.

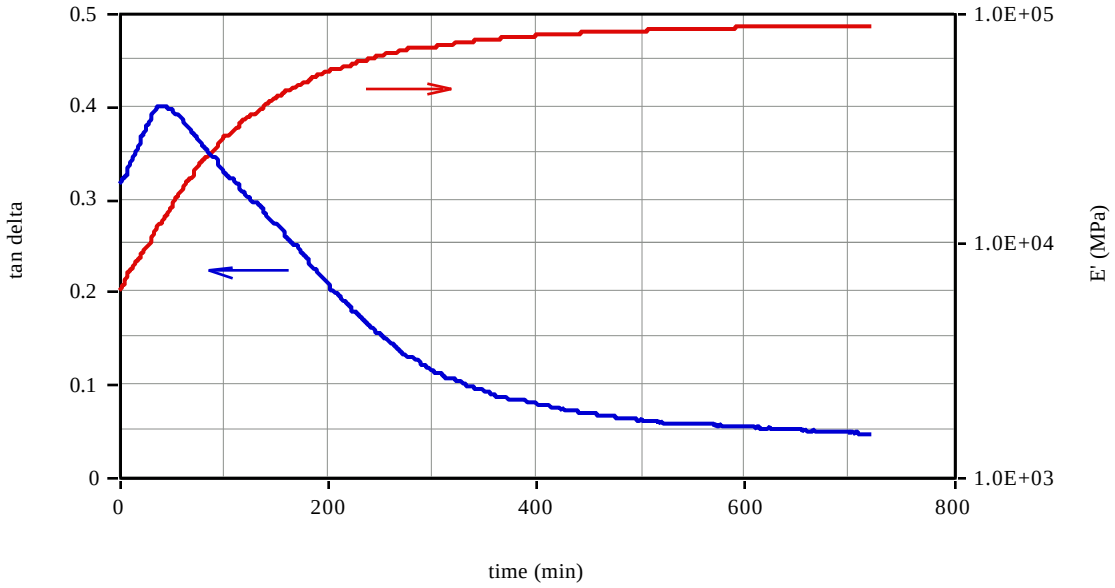

Figure 4-19. Loss tangent (tan delta) and storage modulus (E') for curing Devcon Two-Ton epoxy, as measured at 1 Hz using a Netzsch DMA instrument, at 25°C.

Isothermal DMA tests performed on the RTM-1 were conducted on the Rheometrics 800 mechanical spectrometer until the instrument began shaking when the storage modulus exceeded the machine's capacity. The data, reproduced in Figure 4-22, shows that at approximately thirty-five minutes into the test the magnitude of the storage modulus exceeded that of the loss modulus. For the first twenty-two minutes of the test, the value of G' was below the resolution of the spectrometer, and was therefore not plotted on the logarithmic scale of Figure 4-22.

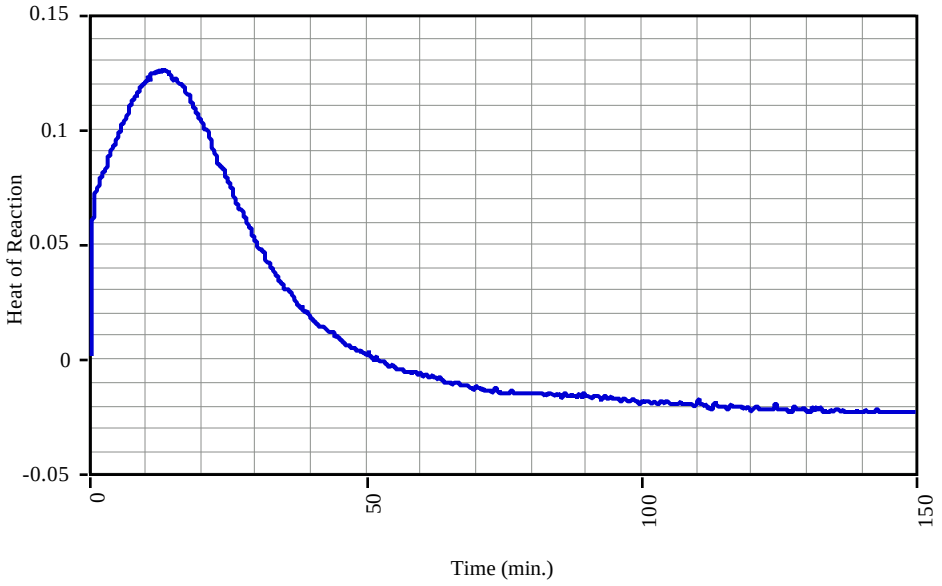

Figure 4-20. Isothermal differential scanning calorimeter scan of RTM-1 epoxy.

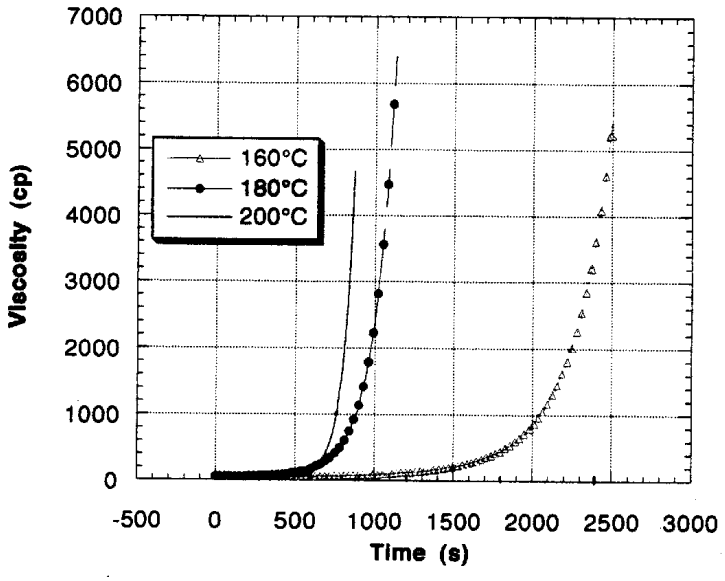

Figure 4-21. Viscosity measurements of RTM-1 epoxy during cure at 160°C, 180°C, and 200°C.

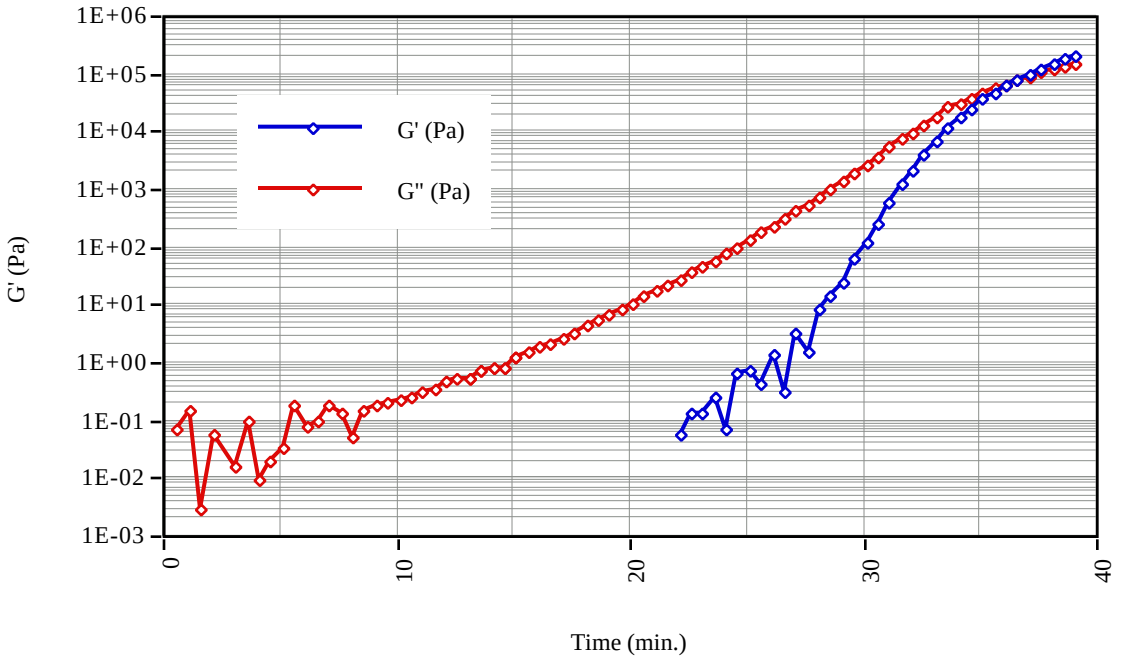

Figure 4-22. Dynamic mechanical analysis results for RTM-1 epoxy during cure at 180°C, using a Rheometrics 800 mechanical spectrometer at 0.16 Hz excitation with variable strain.

The loss tangent, calculated by taking the ratio of the two curves in Figure 4-22, is depicted in Figure 4-23 for those time periods in which a finite value for the ratio results. The scatter in *G'* for low values of the modulus early in the cure contributes to some scatter in the loss tangent, but the trend is clearly decreasing, and the point at which $\tan \delta = 1$ (or equivalently, when G' = G") is seen to occur at about 38 minutes. As noted in Section 2.1, the point at which $\tan \delta = 1$ has been proposed as one criterion for gel point.

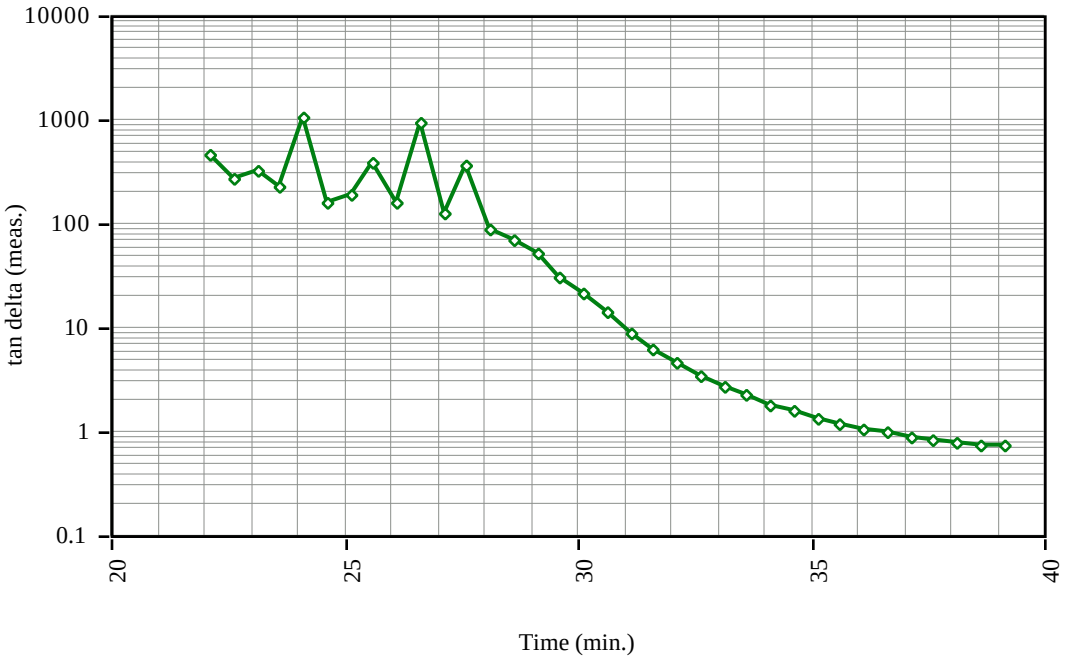

Figure 4-23. Loss tangent (tan δ) for RTM-1 epoxy curing at 180°C, as measured by Rheometrics 800 mechanical spectrometer at 0.16 Hz.

To extend the DMA measurements of the RTM-1 resin to the early stage of cure when the viscosity is low, the curing resin was characterized using a Netzsch DMA 242 dynamical mechanical analyzer operated in the dual cantilever mode using a customer sample holder. The results for the test are shown in Figure 4-24, where the excitation frequency was 10.0 Hz.

As explained in Section 2.2, an epoxy cured at temperatures less than the maximum glass transition temperature $T_{g\infty}$ but greater than the gelation glass transition temperature T_{gg} will exhibit transitions associated with both gelation and vitrification. In Figure 4-24, the first transition at twenty minutes from the start of cure corresponds to gelation. The second transition, at forty minutes, corresponds to vitrification of the polymer. The onset of elasticity is coincident with gelation, as seen in the plot of the absolute shear modulus $|G^*|$, which begins increasing twenty minutes into the cure. The attainment of the maximum modulus occurs approximately forty minutes after the occurrence of the loss peak associated with vitrification.

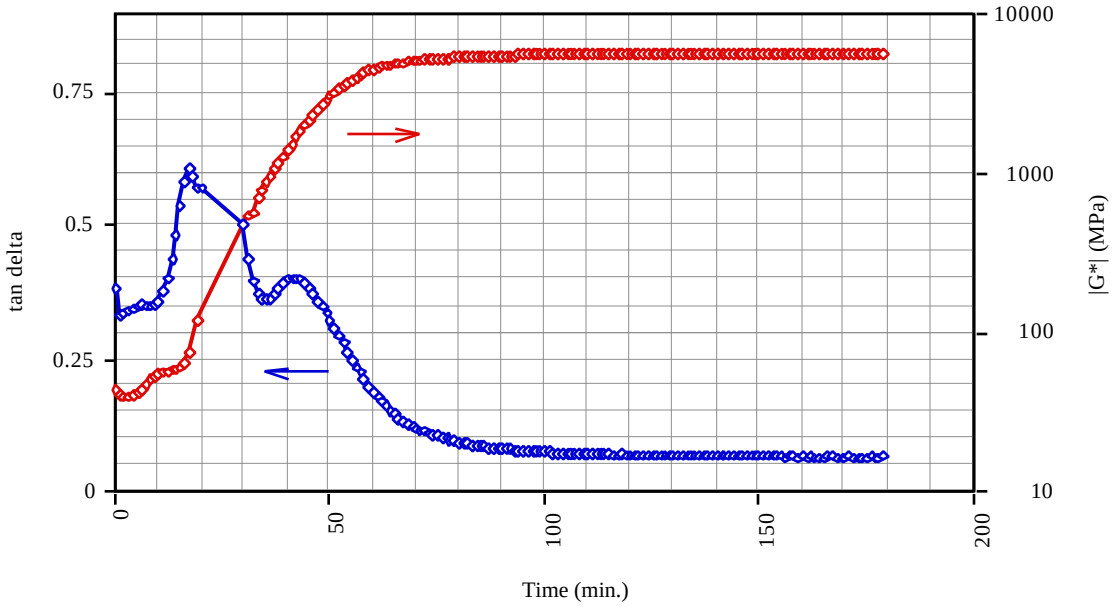

Figure 4-24. Measurements of loss tangent (tan delta) and absolute shear modulus (|G*|) obtained with Netzsch DMA 242 for RTM-1 resin cured at 180°C.

Figure 4-25 shows the measurements at four frequencies of loss tangent for RTM-1 during the same experiment, in which the resin was cured at 180°C. The data show that the times to the gelation and vitrification transitions are slightly shortened for higher frequencies. In accordance with the mechanics of viscoelastic materials, the storage and loss moduli are both increased with higher frequencies, so that the moduli curves and loss tangent curves are effectively shifted to shorter times for higher frequencies as the resin cures.

4.3.2 Evaluation of prototype sensors

4.3.2.1 Evaluation of sensors in Devcon Two Ton epoxy

Prototype sensors were constructed and immersed in curing Devcon Two-Ton epoxy and RTM-1 epoxy to determine if the sensors' outputs varied in a manner that could be correlated with changes in the rheology of the resins. Each sensor was fabricated by attaching an EFPI fiber optic strain gage to an electroded 15 mm x 5 mm x 0.18 mm lead zirconate titanate (PZT) plate using small dots of epoxy to attach the input and reflector fibers to the PZT plate as shown in Figure 3.1. The epoxy used to attach the fibers was a

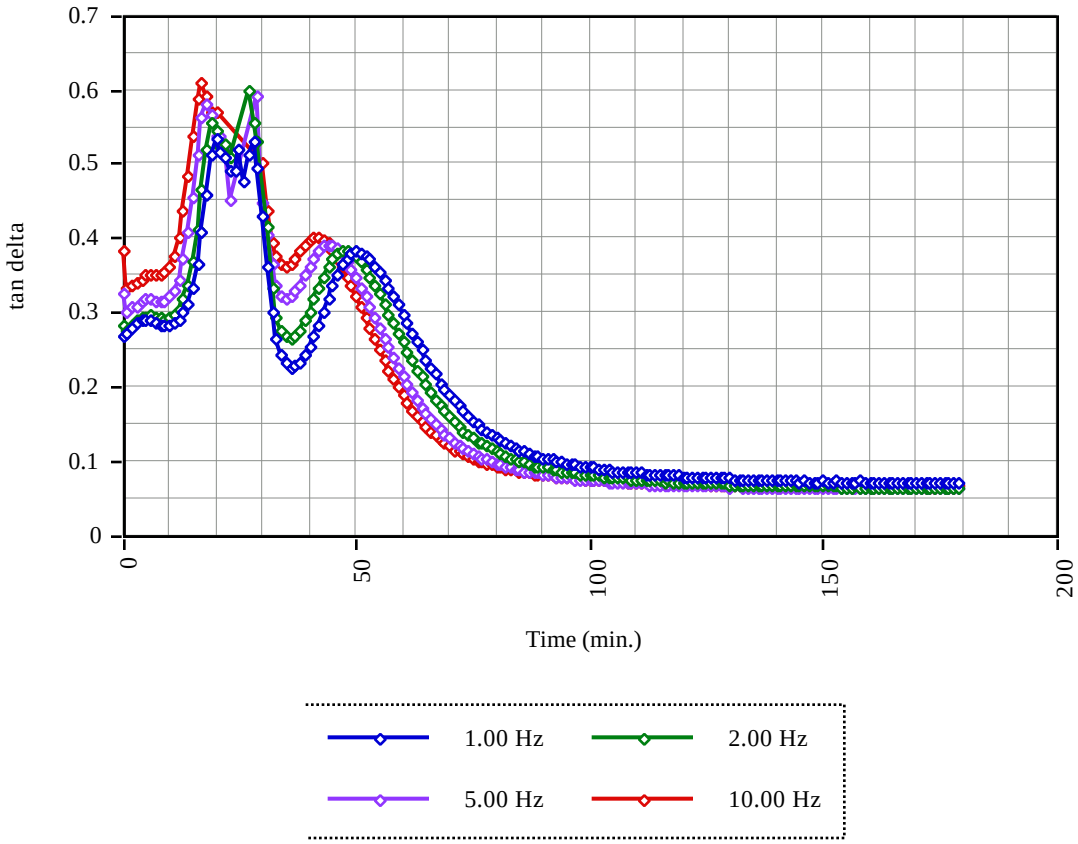

Figure 4-25. DMA measurements of loss tangent (tan delta) at four frequencies for RTM-1 resin cured isothermally at 180°C.

Dow Chemical D.E.R. (R) 332 Epoxy based on a diglycidyl ether of bisphenol A and cured with a triethylenetetramine curing agent. The resin was filled with fumed silica to 67% by weight to increase the modulus of the cured epoxy. The epoxy was cured at 200°C for one-half hour, and was measured to have a glass transition temperature of 140°C by DSC following cure.

The reflector and input fibers were bonded to the glass capillary tube by Dow Corning 100% Silicone Sealant, a room temperature vulcanizing silicone elastomer, which was cured at room temperature overnight, and then post-cured at 200°C for one-half hour when the epoxy attaching the EFPI strain gage to the actuator was cured. The mechanical properties of the cured silicone rubber were determined by DMA, and the results are reproduced in Figure 4-26. Electrical wires (34 AWG) insulated with a polyurethane enamel were bonded to the electrodes using conductive epoxy. The electrodes had been deposited by the PZT

manufacturer using an electroless nickel plating process; each electrode covered one of the two broad sides of the actuator.

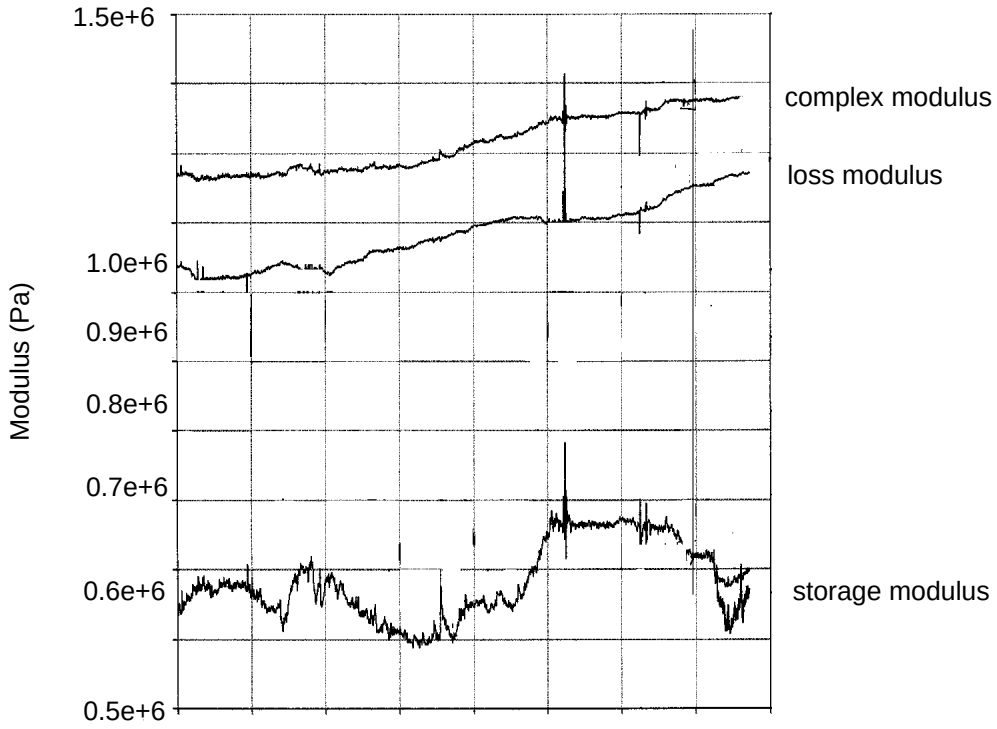

Figure 4-26. DMA measurements of the Dow Corning silicone rubber used to seal the reflector and input fibers to the EFPI capillary alignment tube.

The set-up illustrated in Figure 4-6 was used to acquire data, except that the thermocouple was not attached to the actuator, but was instead suspended in the curing epoxy. A program written using LabVIEW® was used to interrogate the lock-in amplifier through the GPIB interface to determine the phase and amplitude, and to measure the resin temperature using a thermocouple and an analog-to-digital (A/D) card. The LabVIEW® program, or virtual instrument (VI), displays the temperature, phase, and amplitude in a scrolling chart for

monitoring during the test, and stores the data in a spreadsheet file for later analysis.[41] The documentation for the LabVIEW virtual instrument is presented in Appendix C.

To test the use of the sensor in an application with well defined actuator-boundary separations, a sample of freshly mixed Two-Ton epoxy was cured in the adjustable boundary apparatus described in Section 4.2 (Figure 4-3). A prototype sensor was attached to a 1-mm diameter, 10 cm long rod, so that the sensor could be fixed inside the apparatus cavity. The micrometers were adjusted so that the actuator-boundary separation was 2.5 mm on both sides of the sensor.

For all tests involving Two-Ton epoxy, 10 grams of epoxy were mixed for twenty seconds in a fresh container with 8 grams of hardener, according to the manufacturer's recommendation. The freshly mixed resin was poured into the vessel containing the sensor and thermocouple, and the automated data collection was initiated.

Figure 4-27 displays the record of the resin temperature measured by the embedded thermocouple over the duration of the twelve hour test. As the plot shows, the peak exotherm had already passed by the time the data acquisition was started. On the same figure, the phase output of the lock-in amplifier for excitation at 0.5 Hz is superimposed over the temperature profile. Two local maxima were observed, corresponding to gelation followed by vitrification.

The loss tangent at five excitation frequencies is shown in Figure 4-28. The loss tangent was calculated by taking the phase output of the lock-in amplifier at the five frequencies, and subtracting any constant offsets, in order to equalize the starting phase at all frequencies. Taking the tangent of the resulting equalized phase data resulted in the plots seen in Figure 4-28. As the data show, the gelation and vitrification transitions are shown to shift to earlier times for higher frequencies, in keeping with the shift to higher moduli values at higher frequencies.

[41] National Instruments, 6504 Bridge Point Parkway, Austin, TX 78730-5039.

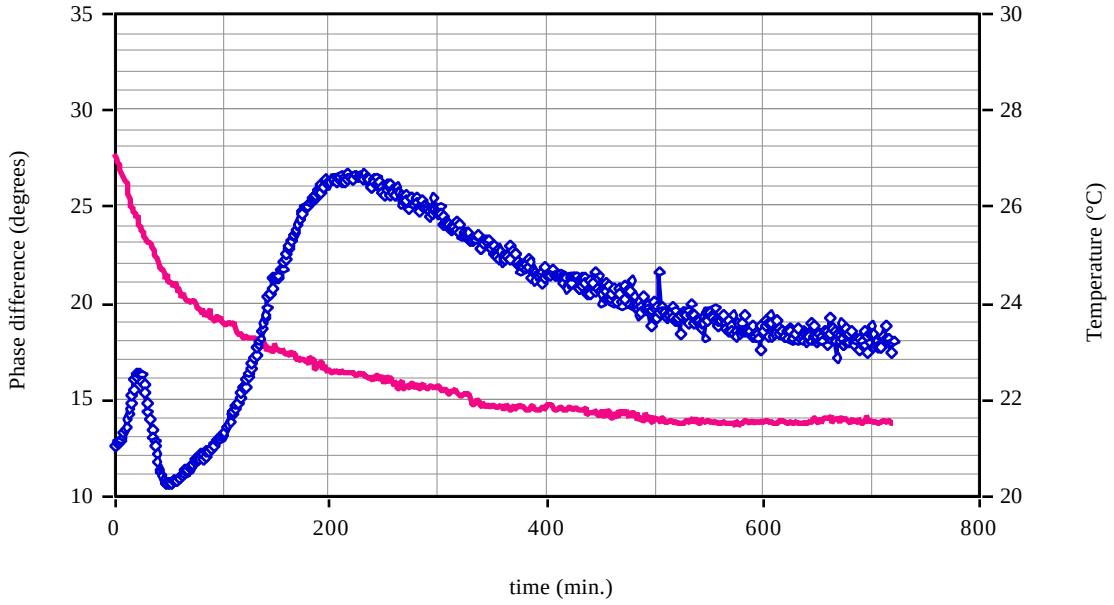

Figure 4-27. Plot of temperature and phase difference between sine output of lock-in amplifier and strain signal output by absolute fiber sensor system, for Devcon Two-Ton epoxy cured at room temperature, for 0.5 Hz excitation.

The strain signal amplitudes as measured by the lock-in amplifier are plotted in Figure 4-28. Two sharp decreases in strain amplitude are detected; the first associated with gelation, and the second with vitrification. Applying Equation 33 to the strain amplitude data, with the boundary separation value *c* set to 2.5 mm, the absolute shear modulus is calculated. Figure 4-29 illustrates the calculated change in absolute shear modulus at 0.5 Hz, displayed on a logarithmic plot, superimposed on the loss tangent measurement for that frequency. The figure shows that the changes in shear modulus are consistent with the peaks in the loss tangent indicating gelation and vitrification.

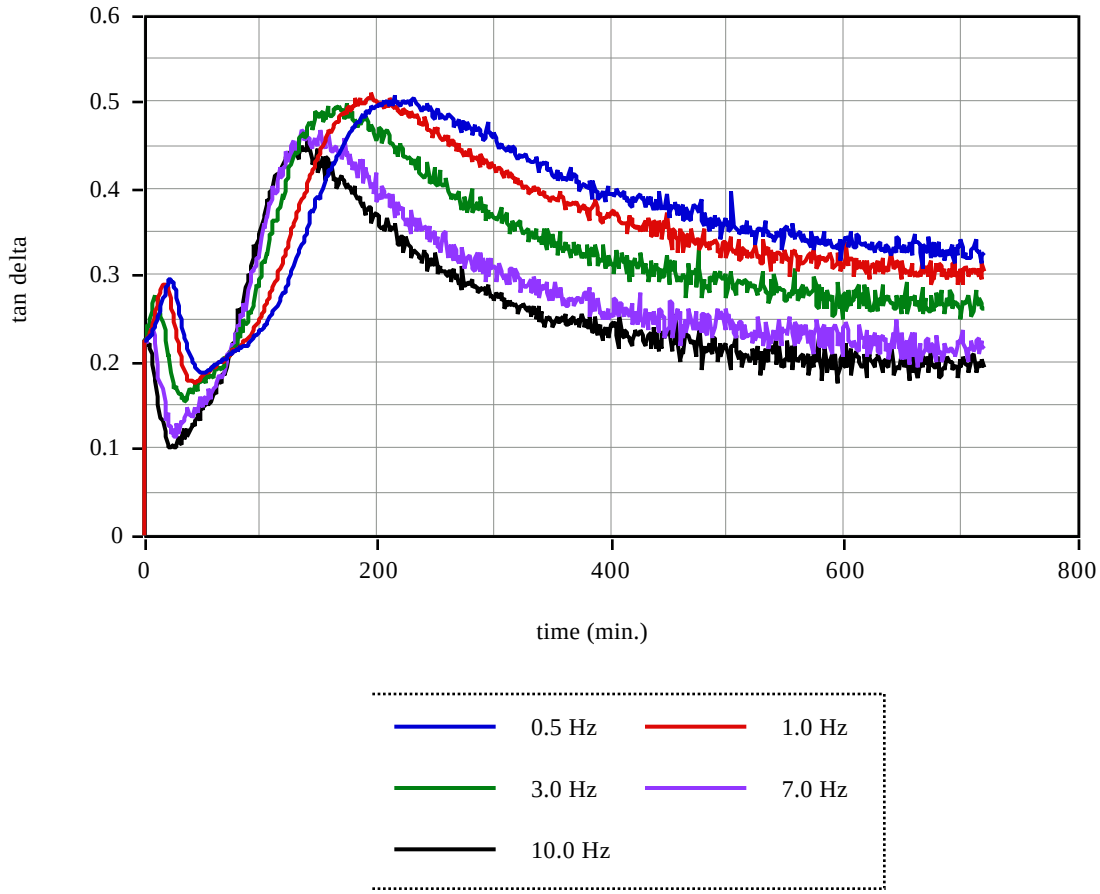

Figure 4-28. Loss tangent for curing Two-Ton epoxy at five excitation frequencies.

A series of tests of prototype sensors in curing Two-Ton epoxy was undertaken to assess the repeatability of the sensor. For each test, the sensor was placed in the bottom of a two inch diameter plastic dish, using a small wooden shim under the input fiber to elevate the sensor from the dish bottom by 1.0 mm ± 0.3 mm. Since the separation of the boundary (dish bottom) from the actuator was not strictly controlled, absolute values of the complex modulus of the resin could not be determined from the output data. Instead, the data were used to determine if the change in phase difference φ and strain amplitude could be observed to change with cure. Data acquisition for each test was terminated at sixty minutes (these tests were performed early in the research, and the existence of the vitrification transition at times greater than sixty minutes had not been identified).

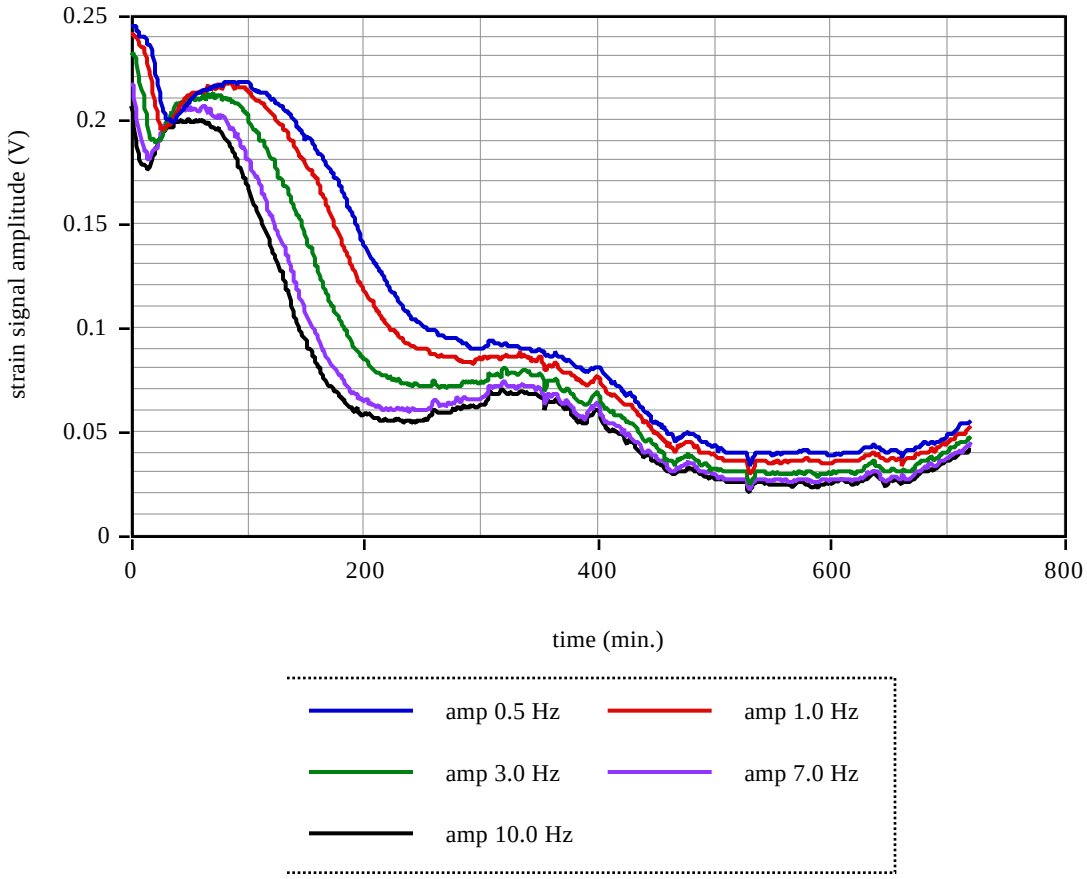

Figure 4-29. Strain signal amplitude output by lock-in amplifier for curing Two-Ton epoxy at five excitation frequencies.

The results of nine tests, each with an unbounded prototype sensor constructed as in Figure 3-1 and immersed in approximately two cm^3 (18 g.) of freshly mixed (10:8 epoxy:hardener) Two-Ton epoxy are summarized in Figure 4-31 and Figure 4-32. As seen in Figure 4-30, the measures of tan delta, calculated by taking the tangent of the phase difference between the electrical excitation and the strain sensor output, agree generally with the Rheometrics DMA characterization of Two-Ton epoxy. The output is observed to remain approximately constant for the first twenty to twenty-five minutes of the test, although some samples an initial increase in tan delta was followed by a slight decrease. As explained later, this increase appears to be due to the sensitivity of the PZT actuator's electrical impedance to the rise in temperature from the reaction exotherm. Following an unequivocal rise in tan delta after twenty to twenty-five minutes, most tests demonstrated a maximum in the output of the phase, followed by a slight decrease. The tan delta maximum, which occurred anywhere

from twenty-five minutes to fifty minutes, appear to correlate with the maximum of tan delta measured by DMA, since most tests resulted in tan delta maxima around thirty-five to forty minutes from the start of the test.

Figure 4-30 summarizes the trends in the amplitude of the voltage output of the FOSS-II sensor processing system, which is proportional to strain. For most of the sensors tested, the strain signal amplitude is approximately constant, until a marked decrease in amplitude is observed anywhere from fifteen minutes to thirty-five minutes into the test. Three of the sensors (sensors 17, 18, and 19) displayed a dip in signal amplitude centered approximately 15 minute after the start of the test. In each of these cases, the amplitude recovered to its original value, before the subsequent final decrease in amplitude was noted. Support for the possibility that these temporary dips in amplitude are associated with the temperature of the resin is given below. The spread in the point in time at which the final

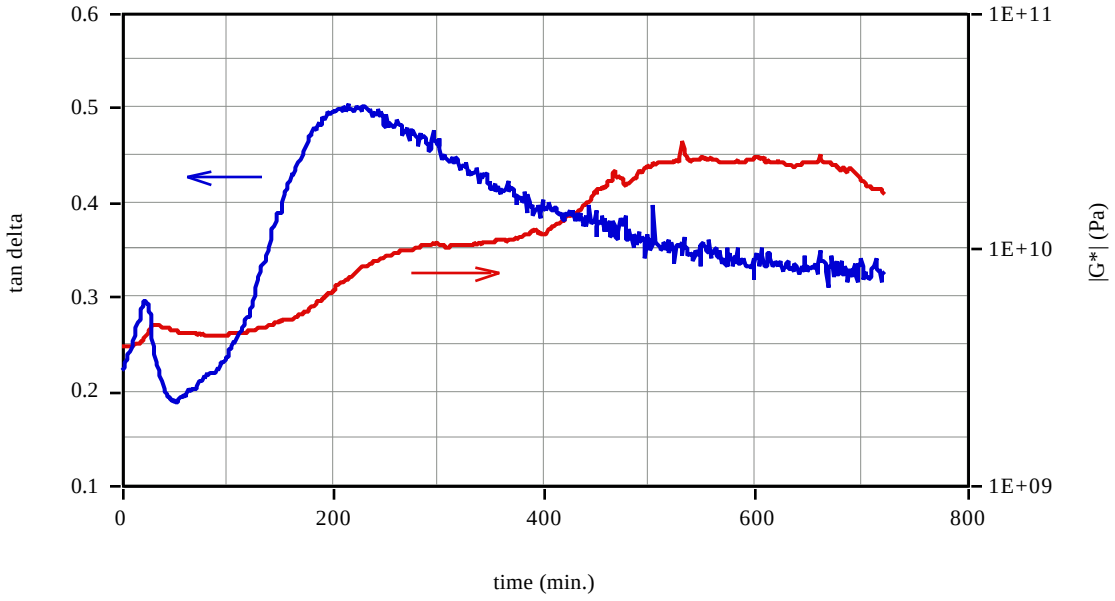

Figure 4-30. Loss tangent (tan delta) and absolute shear modulus |*G**| for curing Two-Ton epoxy at 0.5 Hz. The absolute shear modulus was calculated from the strain signal amplitude in Figure 4-28, using Equation 33.

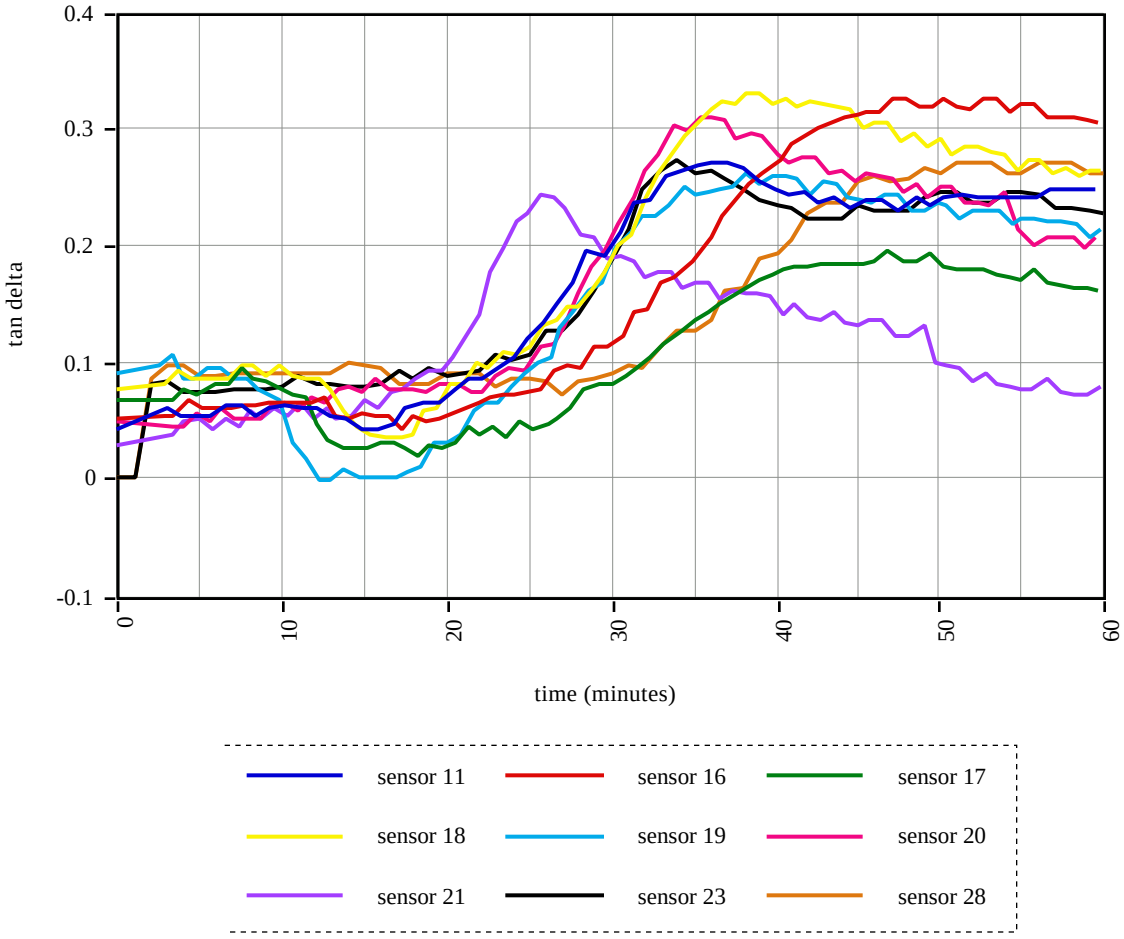

Figure 4-31. Summary of phase outputs, reported as loss tangent (*tan* δ), for nine tests of different prototype unbounded sensors, each in Devcon Two-Ton epoxy cured at room temperature.

decrease in strain amplitude begins may possibly be attributed to variations in the proportion of the resin and hardener used for the test. In general, the sensors which demonstrated an early drop in amplitude also showed and early increase in tan delta, and similarly, those that showed a late drop in amplitude had a late increase in tan delta.

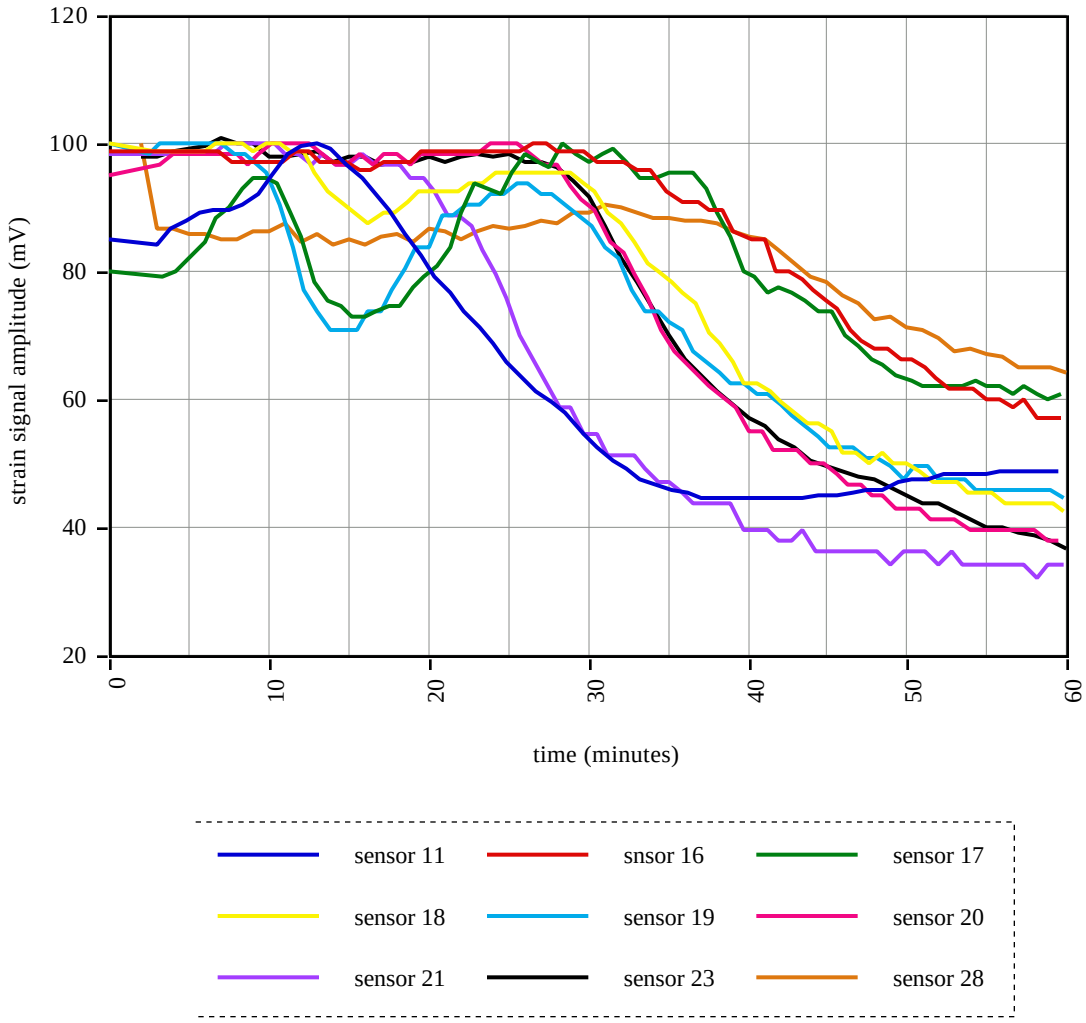

Figure 4-32. Summary of Strain signal output amplitude for nine tests of different prototype unbounded sensors, each in Devcon Two-Ton epoxy cured at room temperature. Units are in millivolts, which are proportional (but uncalibrated) to strain.

4.3.2.2 Evaluation of sensors in neat RTM-1 epoxy cured at 180°C

The test procedure for evaluation of prototype sensors in RTM-1 epoxy was similar to that used for Devcon Two-Ton epoxy, with the principal difference that accommodations were made to heat the resin to promote the cure. For each test, a sensor was fixed to a two inch diameter disposable aluminum dish using polyimide-backed adhesive tape, with a 2.0 mm thick wooden shim under the input fiber to elevate the sensor from the bottom of the dish.

A thermocouple was also attached to the dish using polyimide tape, for monitoring of the epoxy temperature. At room temperature, the viscosity of the uncured resin is sufficiently high to prohibit pouring. The resin was therefore heated to approximately 90°C using an infrared heat lamp, at which point the resin viscosity dropped to about one Pa·s, permitting the resin to be poured into the dish. After approximately two cubic centimeters of resin was poured into the dish, covering the sensor, the dish was placed in a small enclosed oven preheated to 180°C. At this point, the automated data collection using the LabVIEW software was started.

For the first four sensors tested in RTM-1, strong output signals with strain amplitudes on the order of 50 to 300 microstrain were recorded for temperatures less than 100°C. The actual amplitude of actuator motion was approximately one to four micrometers of extension in the fifteen millimeter long actuator. However, for temperatures greater than about 100°C, the strain amplitude dropped suddenly to no more than 10 microstrain. In order to investigate the cause for this effect, a prototype sensor was fabricated using a resistive foil electrical strain gage to substitute for the fiber optic strain gage, with a strain gage bridge to substitute for the optoelectronic support unit. Again, the strain amplitude dropped precipitously when the resin temperature exceeded 100°C. This result appeared to rule out the optical fiber strain gage as a factor in the decreased sensor output.

During the sixth test undertaken with a prototype sensor, the frequency of excitation was reduced to 0.1 Hz in order to investigate the role of frequency in the effect. When the temperature exceeded 165°C, the strain amplitude again dropped. At this time, small flashes of light were observed in the resin sample, at a frequency of 0.1 Hz, in the vicinity of the actuator. Since this indicated the possibility that the resin was shorting the high voltage (150 V peak) applied to the actuator at high temperatures, the voltage output by the high voltage amplifier was monitored using an oscilloscope with a high input impedance. The output voltage was found to be 150 $V_{0\text{-}p}$ for temperatures below approximately 165°C, and less than 2 $V_{0\text{-}p}$ for temperatures above 168°C, confirming that the actuator was shorting out. Since the electrode separation on the sides of the actuator are only 0.19 mm, a peak electric field on the order of 750 kV/m will exist on the periphery of the actuator. It appears that this field is sufficiently high to induce dielectric breakdown of the resin at high temperatures.

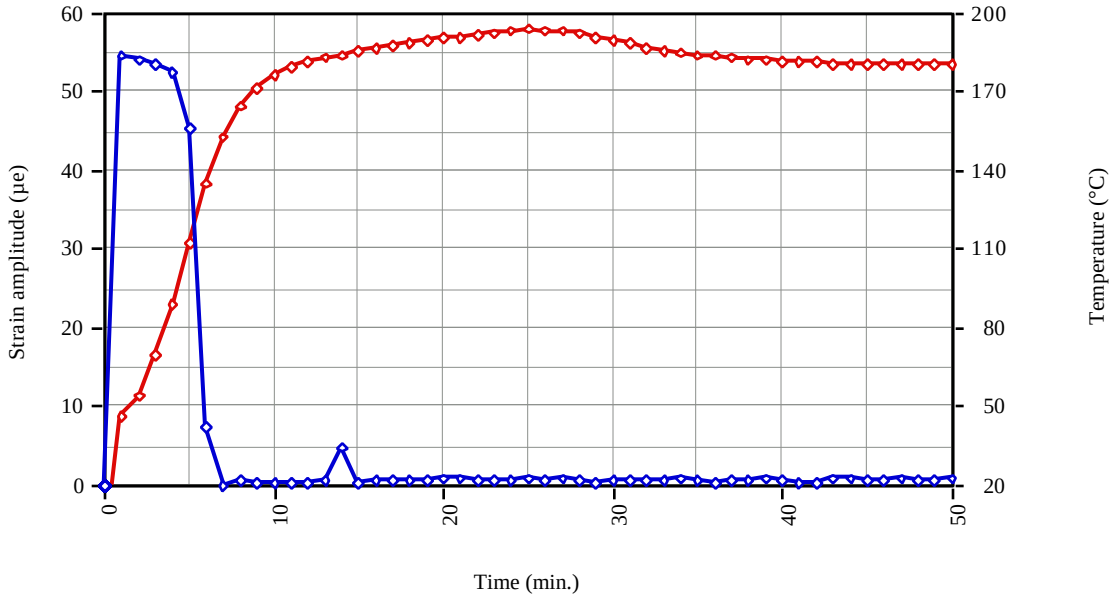

Figure 4-33. Strain amplitude output of sensor in curing RTM-1 epoxy, showing drop in amplitude at temperatures greater than 100°C.

Independently, the DC resistivity of curing RTM-1 resin was measured as a function of temperature by engineers at Bell Helicopter Textron, Ft. Worth, TX, using a mega-ohmmeter. At 93°C (200°F), the resin was measured to have a DC resistivity of 140 MΩ·m, decreasing to 10 MΩ·m at 121°C (250°F), and reaching a minimum of 5 MΩ·m at 165°C (330°F). This result is consistent with the possibility of avalanche breakdown in the epoxy. At the peak AC voltage and the minimum resistance, a current of as much as 30 mA result across the electrodes through the resin. The current may possibly ionize the atoms in the polymer, further reducing the resistance, and permitting the current to avalanche, until the voltage returns to zero.

In order to eliminate the shorting of the resin, a passivating layer of silicon dioxide was applied to all subsequent actuators before the fiber strain gage was attached. Based on the dielectric breakdown strength of amorphous silicon dioxide which is estimated to be 900 kV/mm, it was calculated that a passivation layer of greater than 0.3 μm should be sufficient to eliminate the shorting.[42] Accordingly, Advanced Coating Technology of Radford, VA,

[42] W.D. Kingery, H.K. Bowen, and D.R. Uhlmann, *Introduction to Ceramics*, Wiley-Interscience, New York, 1976, pp. 961-963.

was contracted to apply one micron thick silicon dioxide coatings on several 15 mm x 5 mm x 0.19 mm PZT plates by reactive sputtering.[43]

Tests of prototype sensors constructed with passivated actuators showed no signs of shorting when immersed in curing RTM-1 heated at temperatures up to 200°C. Tests were conducted by immersing the sensors into RTM-1 resin, and heating the resin to 200°C. In these cases, the sensor outputs showed the expected change in phase and amplitude up to about 175°C, at which point the sensor output signal decreased sharply. Tests showed that the sensor outputs contained spurious harmonics above 175°C, which were apparently preventing the lock-in amplifier from properly tracking the signal. Since the electrical signal applied to the actuator is a pure sinusoidal function of time, we expect and usually observe that the mechanical strain developed in the actuator is also a pure sinusoid (although delayed in phase and attenuated in amplitude by the viscoelastic resin). However, for temperatures above 175°C, the measurement of the mechanical strain showed a complex waveform indicating the presence of higher harmonics.

To investigate this harmonic generation, a prototype sensor was assembled, and heated to 180°C in air in an oven. The same change in strain output waveform was observed at temperatures over 175°C, showing that the RTM-1 resin was not responsible for the effect. Next, an electrical foil strain gage was attached to a PZT actuator, which was then heated in an oven. The results were identical to those obtained with a fiber optic strain gage, implicating the actuator and not the strain gage as the source of the problem.

The manufacturer of the PZT-5A used for actuators suggested that the harmonic output of the signal generator be measured. Although harmonic components in the signal generator may be 20 dB or more down in amplitude from the fundamental frequency, if a resonance in the actuator coincides with a harmonic in the signal generator, the resulting strain amplitude at that frequency will be greatly exaggerated. Since the electrical characteristics of the actuators change with temperature, the resonance may be shifting to lower frequencies as the temperature is increased. If harmonics exist in the output of the signal generator, those with frequencies at a resonance of the actuator may cause observable displacements at that frequency, even if the amplitude of the harmonic in the signal generator output is a small fraction of the amplitude of the fundamental frequency.

Tests were conducted to measure the harmonic content of signal generators used to drive the PZT actuators. Since a spectrum analyzer was unavailable to measure the signal output, a

[43] Advanced Coating Technologies, 7586 Old Peppers Ferry Loop, Radford, VA 24141.

laboratory computer with a data acquisition card was configured to perform spectrum analysis by programming it to perform a Fast Fourier Transform (FFT) in LabVIEW. The results showed that the signal source used for the RTM-1 tests (the internal oscillator in the SR810 lock-in amplifier) was relatively clean, with harmonics at least 60 dB down from the fundamental frequency. A Beckman signal generator that had been used early in the program (but was not used for the RTM-1 tests in question) was shown to have harmonics that were only 35 dB down.

While these results appear to show that the resonances in the actuator are unlikely to cause the decline in signal seen in the experiments, the impedance of several samples of PZT actuators were measured at temperatures up to 180°C. Any resonances would detected by a reduction in the imaginary (reactive) part of the electrical impedance. An HP 4192A low frequency electrical impedance analyzer was used to search for resonances in the PZT actuators as the temperature of the actuator was increased to 200°C. In the test performed, wires were attached to the electrodes of a PZT wafer by conductive epoxy. The wafer was placed in a small laboratory oven, which was programmed to heat the interior to 200°C, and the wires were attached to the input of the HP 4192A impedance analyzer. As the temperature increased, a data acquisition system recorded the impedance over a range of frequencies from 5 Hz to 2 kHz. The results showed that there were no vibrational resonances between 5 Hz and 2 kHz over the temperature range tested, indicating that resonances are not responsible for the observed nonlinearities.

Further testing of a prototype rheometer sensor at elevated temperatures showed that the sensor nonlinearity was due to an increase in the piezoelectric coefficient of the PZT actuator with increasing temperature. At room temperature, the 150 V_{ac} drive voltage applied to the actuator generated 150 microstrain in the actuator. As the temperature applied to the actuator increased, the resulting strain was seen to also increase, although the drive voltage remained the same. For a drive voltage of 150 V_{ac}, the strain saturated and reached a maximum value at 150°C. To eliminate the saturation of the actuator, the drive voltage was reduced to 60 V_{ac}. Using the reduced drive voltage, the actuator was tested at temperatures up to 220°C without any evidence of nonlinearity or strain saturation.

Using the reduced drive voltage, a prototype sensor was tested in neat RTM-1 resin cured at 180°C. Figure 4-34 illustrates the phase delay between the voltage output by the lock-in amplifier and the actuator extension measured by the fiber optic strain gage, for five frequencies between 0.5 Hz and 10.0 Hz. The upper frequency limit was established by the maximum sampling rate of the absolute fiber sensor system, which is currently set at approximately 66 Hz. This limit is fixed by the maximum slew rate of the charge coupled

device (CCD) array used in the spectrometer. The lower frequency limit was determined empirically by measuring the repeatability of the phase output as the frequency was lowered. At frequencies of 0.1 Hz and less, the repeatability decreased sharply, so that 0.5 Hz was adopted as the low frequency limit.

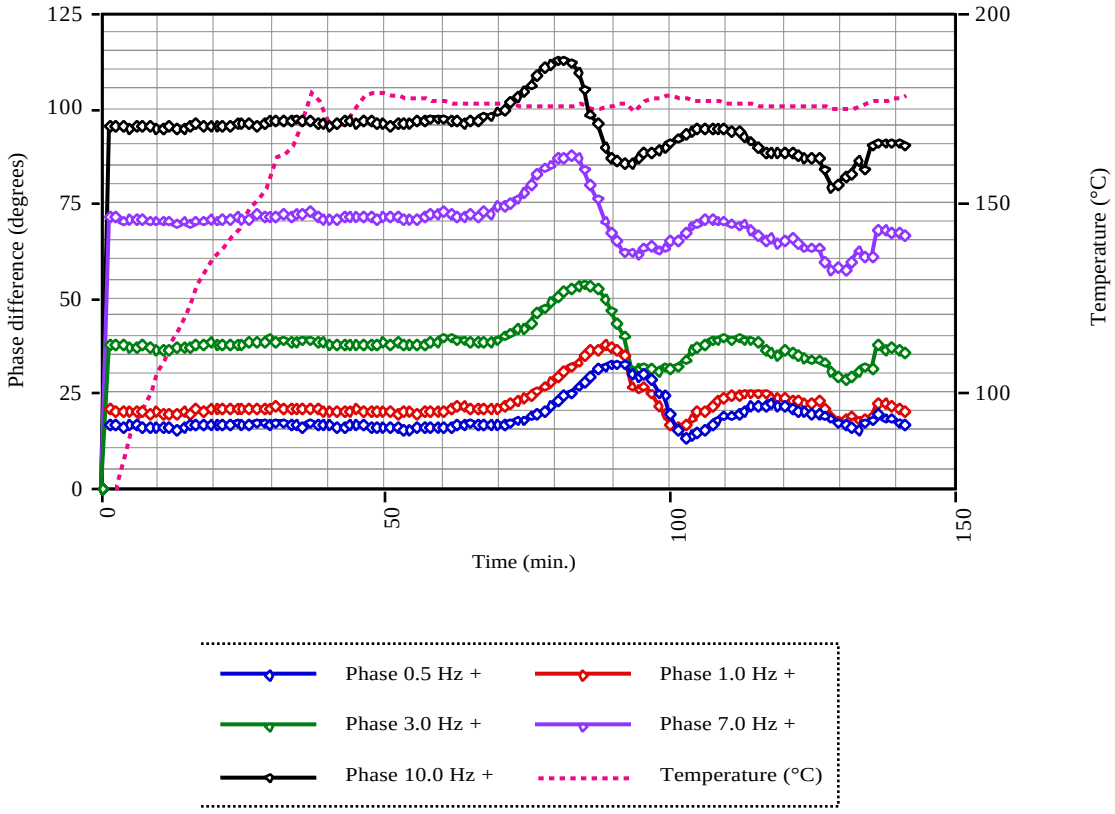

Figure 4-34. Phase output of sensor in neat RTM-1 cured at 180°C.

Figure 4-34 indicates that two loss peaks associated with rheological transitions were observed. This result is consistent with the characterization of RTM-1 using the Netzsch DMA 242 and shown in Figure 4-24. The dependence of the phase output on frequency seen in the figure is a consequence of the variation of both the storage modulus and loss modulus, and of the effect of the frequency dependence of the silicone elastomer used in the sensor construction. To convert the phase measurements to values of loss tangent, the offset of the measurement taken at time t=0 at each frequency was subtracted from the data for the phase difference at that frequency, and then the tangent was calculated from the data with the offset removed. The results, as shown in Figure 4-35, show the same two loss

peaks and reproduce the trend towards earlier maxima at higher frequencies, agreeing with the laboratory DMA results of Figure 4-25. The first peak was observed about forty minutes after the cure temperature reached the maximum value of 180°C.

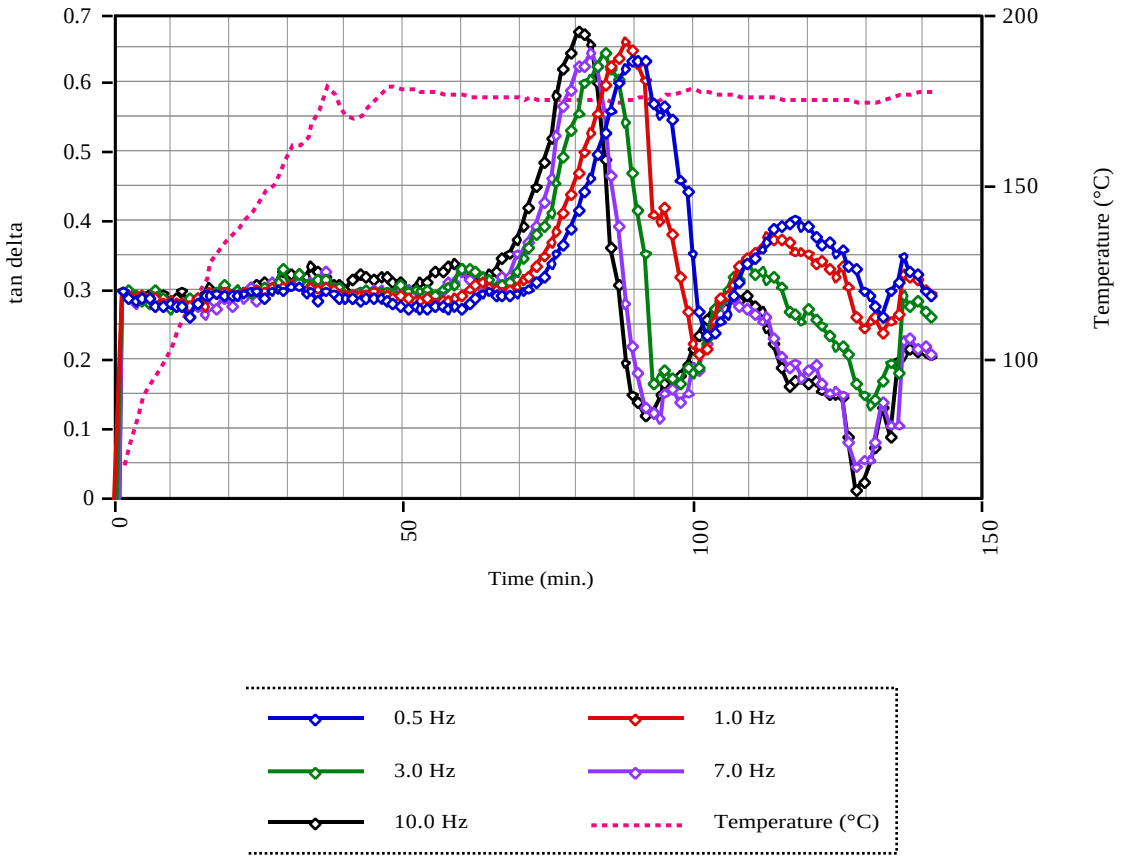

Figure 4-35. Tan delta output of sensor in neat RTM-1 cured at 180°C, with starting phases shifted to equalize tan delta at all frequencies.

The strain amplitude output of the sensor as a function of time for the five excitation frequencies is shown in Figure 4-36. The strain amplitude is seen to decrease at the same time as the first peak in the loss tangent, adding credence to the conclusion that the peak is associated with the loss tangent. Figure 4-37 shows the loss tangent and strain amplitude plotted together for measurements made at 10 Hz excitation, to show the coincidence of the loss peak with the drop in strain amplitude.

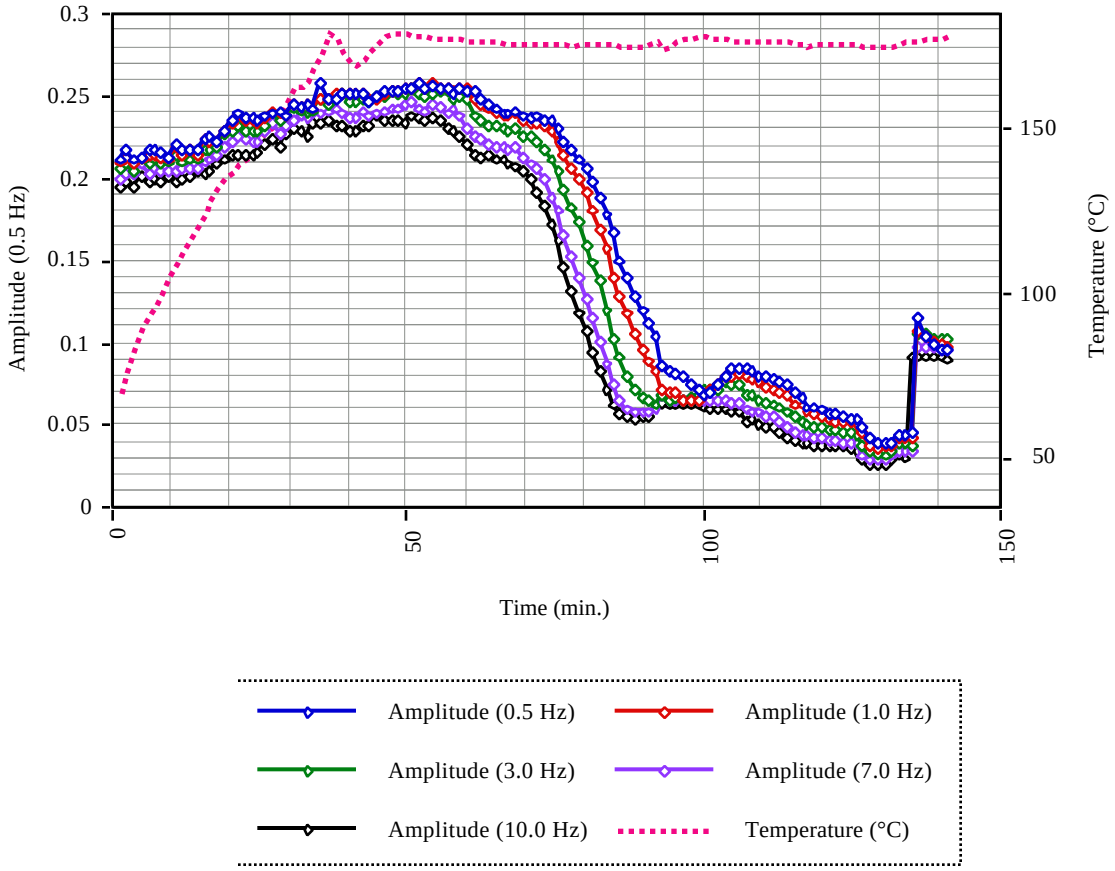

Figure 4-36. Strain amplitude signal output of sensor (as output in volts by lock-in) in neat RTM-1 cured at 180°C.

To convert the strain amplitude data to an approximation of the absolute shear modulus of the epoxy, Equation 33,

$$|G^*| = \left(\frac{c}{2tL}\right)\left(\frac{V_0}{\varepsilon_0}\right)\left(Y_{33}d_{31}\right). \tag{33}$$

was considered. This equation was derived by assuming that the actuator was bounded on two side by fixed, immovable boundaries, separated from the actuator by distance *c*, leading to the geometrical factor for *b* given in Equation 8. For the experiment under

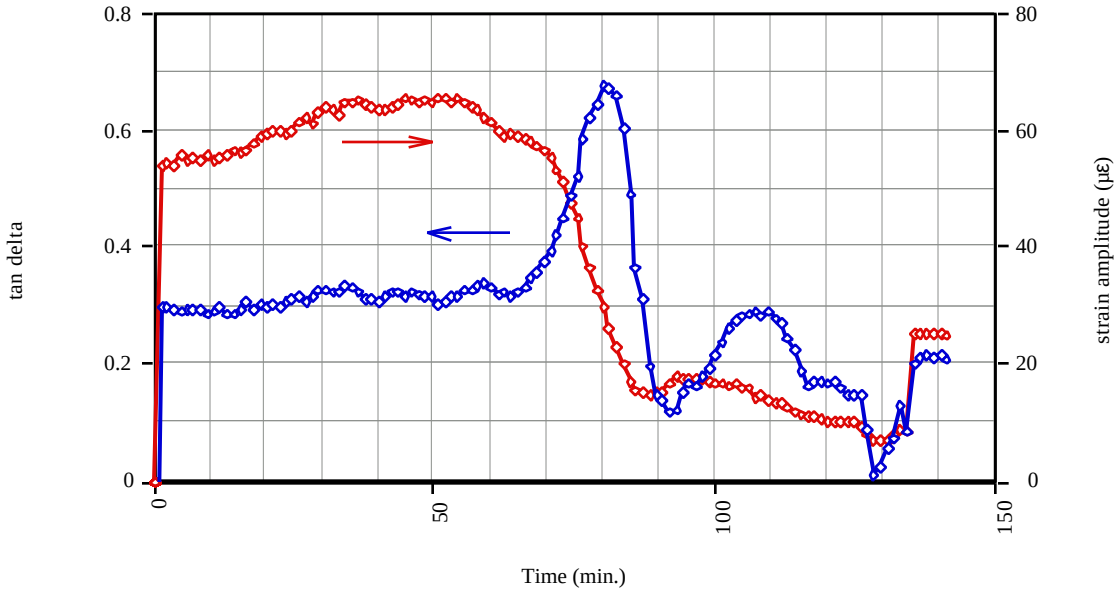

Figure 4-37. Tan delta and strain amplitude output of sensor in neat RTM-1 resin cured at 180°C at 10 Hz excitation.

consideration here, the actuator was separated from a fixed boundary on one side by 2.0 mm, while on the other side, the resin covered the actuator to a depth of approximately 4 mm, with air above the epoxy. In that case, the epoxy is not constrained from moving at the air-epoxy interface, and the separation c_1 of the actuator from the nearest fixed boundary can be considered to be effectively infinity. From Equation 10, the geometrical factor b is given by

$$b = \frac{1}{A}\left(\frac{1}{c_1} + \frac{1}{c_2}\right)^{-1}, \tag{69}$$

so for $c_1 >> c_2$, then

$$b \quad \frac{1}{A}\left(\frac{1}{c_2}\right)^{-1} = \frac{c_2}{A}. \tag{70}$$

The revised equation then becomes

$$\left|G^*\right| = \left(\frac{c_2}{tL}\right)\left(\frac{V_0}{\varepsilon_0}\right)\left(Y_{33}d_{31}\right). \tag{71}$$

In this equation, the contributions to the output from the silicone rubber immitances have been neglected. From the manufacturer's data sheet, the short circuit tensile modulus Y_{33} is $5.3\text{x}10^{10}$ Pa. The piezoelectric coefficient d_{31} was measured to be $2.07\text{x}10^{-10}$, by applying a dc voltage to the actuator in air, and measuring the resulting strain through the use of the attached fiber optic strain gage. The actuator thickness t was 0.18 mm, and the actuator length L was 15 mm. Using those values, the equation relating the absolute shear modulus to the strain amplitude becomes

$$\left|G^*\right| = \frac{3.4x10^5 Pa}{\varepsilon_0}. \tag{72}$$

From this equation and the strain amplitude data of Figure 4-37, the absolute shear modulus at 10 Hz for the RTM-1 resin curing at 180°C was calculated and plotted in Figure 4-38. The ultimate value for the modulus after vitrification is found to be approximately 40 Gpa, which is almost an order of magnitude higher than the value of 5.7 Gpa measured at the end of cure of the RTM-1 sample tested with the Netzsch DMA in Figure 4-24. The reason for this discrepancy is not known at the time of this writing. Part of the discrepancy may be attributed to the variations in the piezoelectric coefficient d_{31} used in the calculation of |G*|. Three samples of the actuators used to fabricate the sensors were tested to determine d_{31}, which varied by 20% over the three samples, from $-1.66\text{x}10^{-10}$ m/V to $-2.07\text{x}10^{-10}$ m/V. The manufacturer's specifications for d31 is $-1.71\text{x}10^{-10}$ m/V.

To derive the values plotted in Figure 4-38, the expression for |G*| which neglects the immitances of the silicone rubber was used. To determine if the mechanical properties of the silicone rubber are partly responsible for the higher values of the modulus at the beginning stages of cure, the contributions to Equation 32 from the silicone rubber immitance terms were figured. From Equation 32, those terms, expressed as a relaxance through the inclusion of the geometrical factor c/A are

$$Q_s(\omega) = \frac{c}{A}\left(E_s + \omega F_s - \omega^2 I_s\right). \tag{73}$$

Note that the factor of 2 premultiplying the actuator area A in Equation 32 has been omitted, in keeping with the new geometrical factor b derived in Equation 70. The inertance I_s was measured in Section 3.3 to be 0.10 ± 0.01 gram. Adopting the values for the elastance and frictance determined in Section 4.2, namely E_s = 6978 Pa-m and F_s = 594.4 Pa-m-s, then the relaxance due to the viscoelasticity of the silicone rubber at 10 Hz is 1.182×10^5 Pa, where the area of the actuator is 7.5×10^{-5} m^2. Clearly this value is much less than the values for the relaxance |G*| calculated using Equation 68, so that the neglect of the silicone rubber terms is justified. It would appear that the silicone rubber properties cannot be used to explain the higher values of absolute shear modulus observed at the end of cure with the prototype sensor.

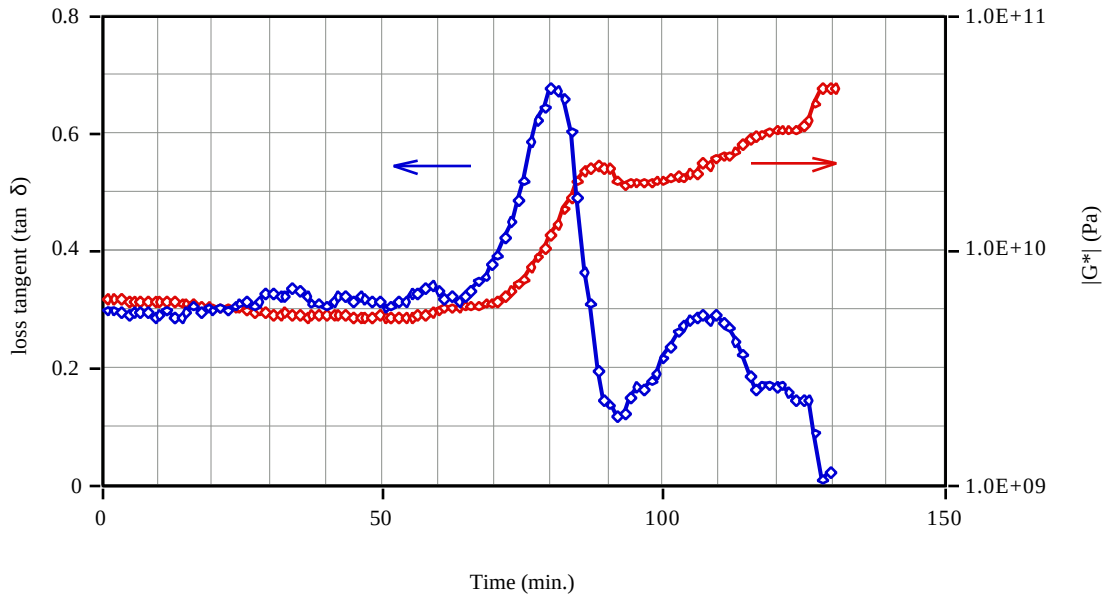

Figure 4-38. Linear plot of loss tangent and log plot of estimated absolute shear modulus |G*| for neat RTM-1 resin cured at 180°C.

4.3.2.3 Evaluation of sensor in curing composite prepreg material

The ultimate practical application for the technology developed here is the monitoring of the changing viscoelasticity of thermosetting resins in composite prepreg material, to facilitate the control of the processing of the material, based on in-situ measurements of material

properties. Towards this end, tests were undertaken to evaluate the use of the sensor in prepreg material, where the reinforcing fibers are impregnated with epoxy resins.

First, prototype viscoelasticity sensors were laid up in 76 mm x 76 mm (3 in x3 in) eight-ply Gr/Ep (graphite fibers in a thermoplastic-toughened epoxy) prepreg laminates to test the use of the sensor in composites processed in a hot press. In these tests, the lay-ups containing the sensors were placed in the hot press, and up to 85 psi was applied to the laminate before the temperature was ramped up to the cure temperature of 176°C (350°F). In the first test, it was found that the graphite fibers shorted out the electrical leads providing power to the actuator. Although the PZT actuator itself had been coated with silicon dioxide for insulation, the insulation had been omitted from the point at which the wires were attached to the actuators using conductive epoxy. In subsequent tests, this attachment point was coated with high-temperature silicone rubber for insulation (after the wires were bonded).

In the next test, the application of pressure from the hot press caused the ceramic PZT actuator to fracture. This appeared to result because the pressure was applied before the viscosity of the resin was reduced by heating of the lay-up. Reduced resin viscosity should allow the resin to flow during application of pressure, permitting the graphite fibers to rearrange themselves around the sensor. Also, the ram pressure had been adjusted to 765 lbf to give 85 psi over the 5,806 square mm (9 square inches) area of the prepreg. However, since the sensor assembly caused the prepreg to bulge over the sensor area, the press first contacted the prepreg exclusively over the sensor, which at first supported the entire 765 lbf, probably leading to fracture of the actuator.

To improve the survival of the actuator during the pressing operation, a sensor was constructed using a THUNDER® actuator. THUNDER® is a piezoelectric actuator developed by NASA Langley Research Center, and constructed by sandwiching a sheet of PZT ceramic with a metal foil on one side, and with a polyimide film on the other. By prestressing the substrate before the PZT wafer is attached, a curvature in the plane of the actuator results, allowing greater out-of-plane mechanical displacements by the assembly than those possible by the PZT actuator alone. In this application, the area of the actuator used was so small that the out-of-plane curvature was negligible. The lamination of the actuation was expected to improve the survival of the PZT during hot pressing. The pressing operation may cause the ceramic to fracture, but it would be held in place by the bonded layers.

In the first test of the sensor with a THUNDER® actuator, the sensor was embedded in an eight-ply Gr/Ep lay-up. The actuator continued to work after pressing of the prepreg at room temperature, although it was found to have delaminated when the uncured prepreg was peeled apart to examine the actuator. The delamination was attributed to improper bonding of the actuator to the metal foil during fabrication of the part at NASA, so a new THUNDER® sample was obtained in order to construct a new sensor.

A new sample of THUNDER® was obtained from NASA, and another sensor was assembled using the new material. Before embedding in prepreg, the sensitivity of the sensor outputs to temperature was evaluated. The sensor was suspended in air in a small oven, and the sensor outputs were recorded as the temperature was increased to 180°C, and then cooled to room temperature. As Figure 4-39 reveals, the phase increased by five degrees as the temperature was increased from 21°C to 180°C, and then decreased by five degrees as the temperature dropped from 180°C to 58°C. By plotting the phase as a function of frequency in the scatter plot of Figure 4-40, an average value of 0.03 degrees (phase) per degree Celsius was estimated for the temperature dependence.

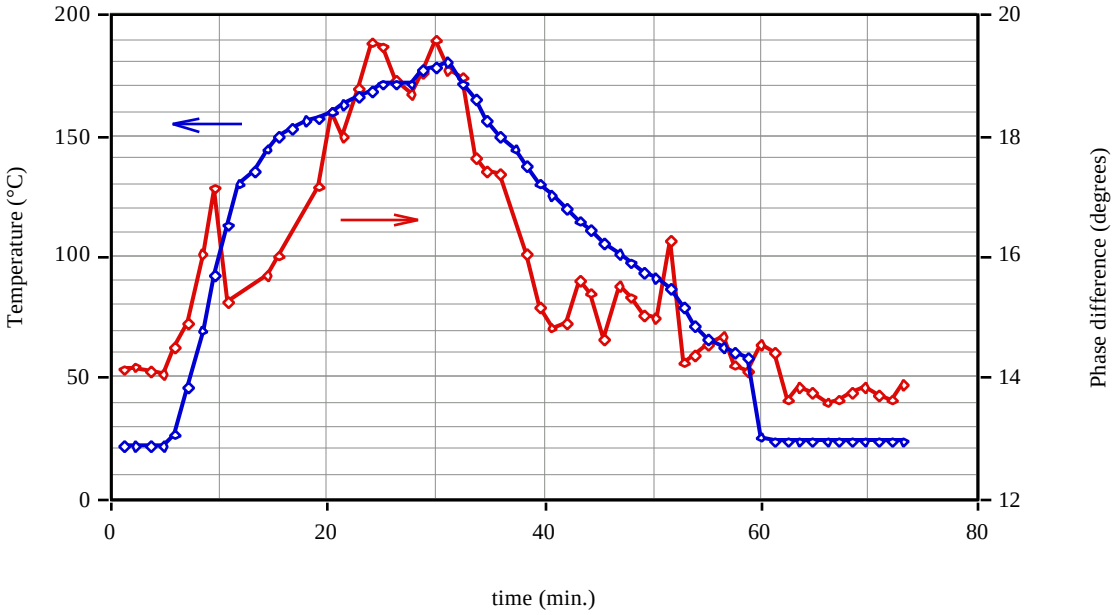

Figure 4-39. Phase shift of signal output by prototype sensor for changing temperature.

During the same temperature test, the change in the strain amplitude signal was recorded. The signal displayed in Figure 4-41 is the voltage output by the lock-in amplifier, which is

the root-mean-square (RMS) value of the sinusoidally varying signal output by the absolute fiber sensor system, which in turn monitors the fiber optic strain gage. As the temperature increased from 21°C to 180°C, the output signal also increased from 239 mV to 347 mV. For the temperature decline from 180°C to 23.7°C, the strain amplitude decreased from 347 mV to 248 mV. A scatter plot of the data with linear least-squares fit is shown in Figure 4-42. Expressed as a percentage, the temperature-induced change in signal amplitude was found to be 0.4% $°C^{-1}$.

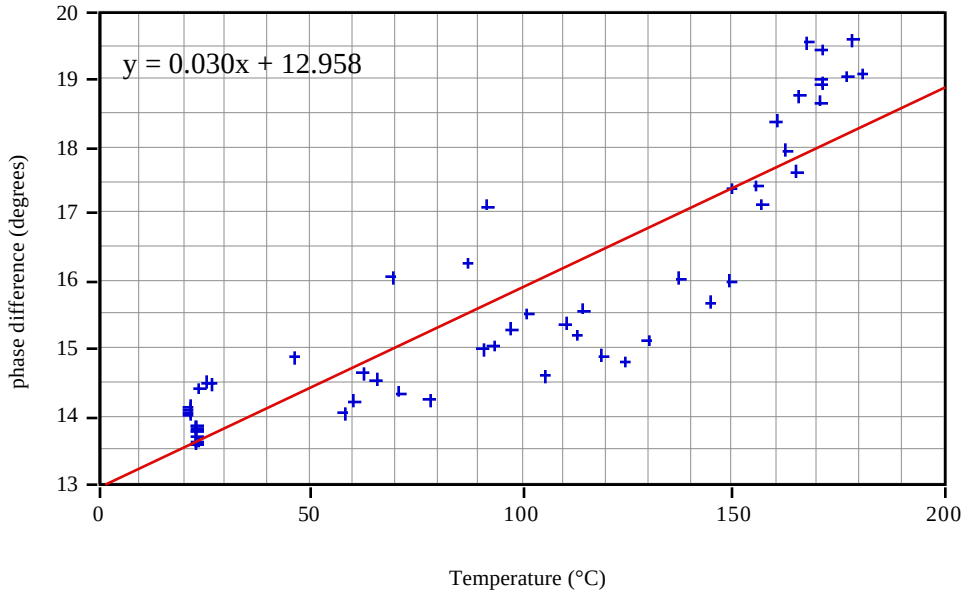

Figure 4-40. Scatter plot of phase difference as a function of applied temperature, and least squares curve fit.

After characterization of the temperature sensitivity, the sensor was embedded in the midplane of a twelve-ply $[0_2/90_2/0_2]_s$ Gr/Ep lay-up, together with a thermocouple to measure the temperature. The lay-up was place in a Carver hydraulically-operated press, and the temperature was increased to 100°C for approximately 40 minutes. After this preliminary temperature soak, a nominal pressure sufficient to permit contact of upper and lower platens to the prepreg was applied, and the temperature was ramped to the final temperature of 180°C. Figure 4-43 reveals that the phase output of the lock-in amplifier at 0.5 Hz (blue trace) shows trends that appear to follow the increase in temperature. By multiplying the change in temperature by the factor (3.5 °phase/°C) derived for the temperature-induced phase shift above, and subtracting the result from the phase

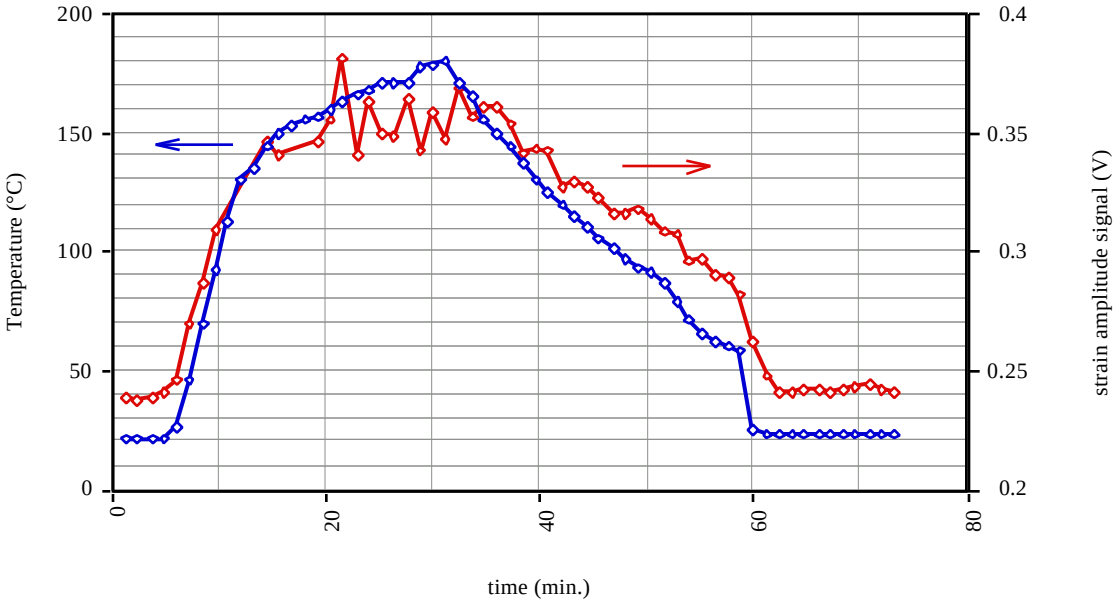

Figure 4-41. Change in strain amplitude signal of prototype sensor for changing temperature.

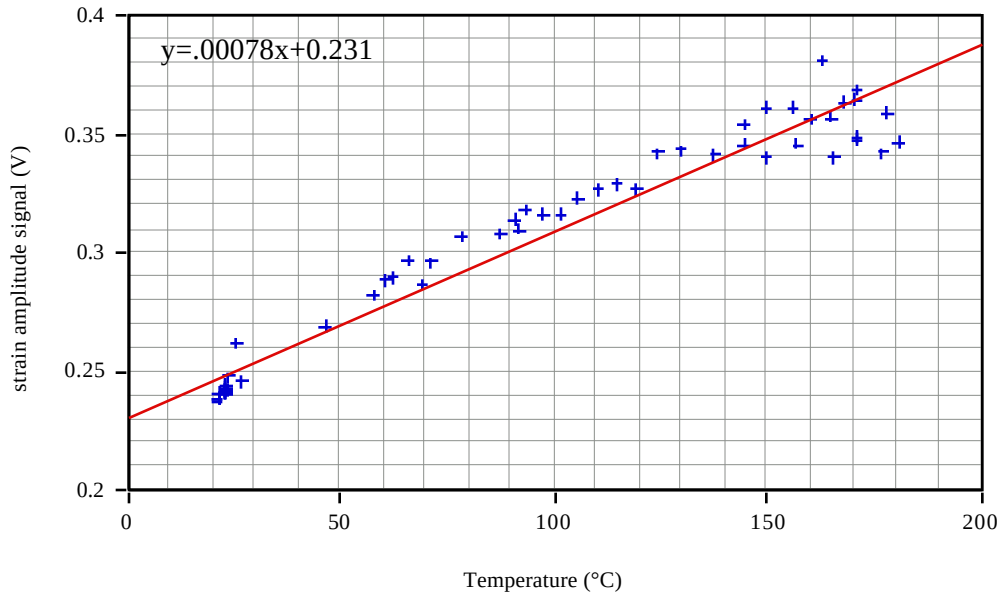

Figure 4-42. Scatter plot of strain amplitude signal as a function of applied temperature, with linear least-squares curve fit.

difference, a temperature-corrected phase difference ensues, shown in red in Figure 4-43. The corrected phase difference holds approximately constant, until a small decrease is followed by a marked increase 140 minutes after the start of the test. The increase is followed by a small decrease before the phase remained relatively constant for the remainder of the test.

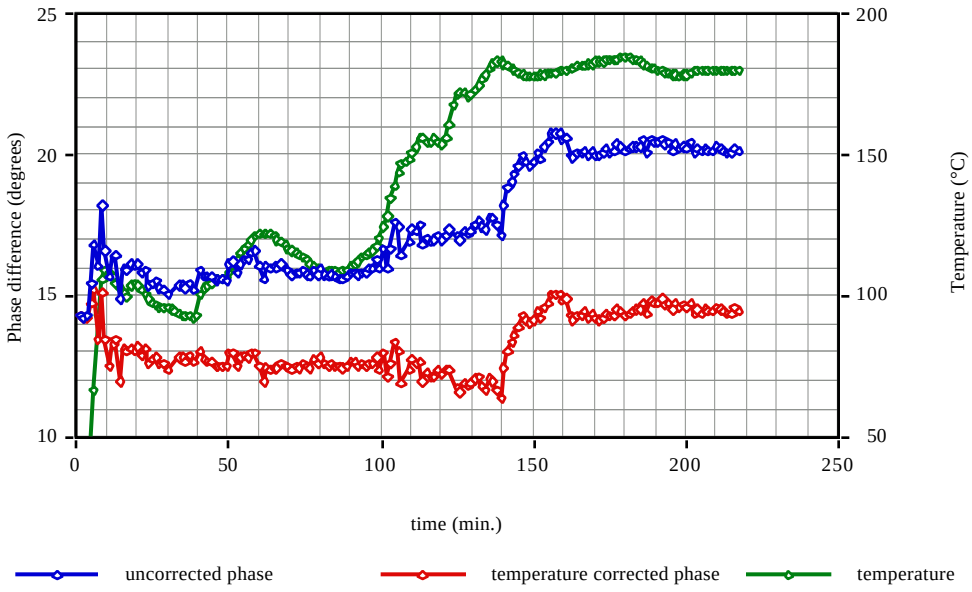

Figure 4-43. Temperature (green trace), phase difference output by lock-in amplifier (blue), and phase difference after subtraction of temperature effects (red).

The strain amplitude signal at 0.5 Hz shows a somewhat stronger correlation with the temperature changes. To derive a version of the signal corrected for the temperature variations, the factor (0.4%/°C) derived for the temperature-induced change in signal was multiplied by the change in temperature, and then this result was in turn multiplied by the uncorrected signal. This result, which yielded the variation due to temperature, was subtracted from the uncorrected signal to give the final temperature-corrected signal in Figure 4-44. Despite some jumps in the data, it can be seen that the trend indicates that the strain amplitude is relatively constant up to 100 minutes into the test, at which point it decreases over the next fifty minutes.

The jumps in the strain amplitude data also suggest that slip-stick behavior may be influencing the output of the sensor. In the slip-stick phenomenon, the traction between the sensor and the adjacent resin is suddenly released as the surface adhesion fails, so that the

sensor motion is no longer constrained by the resin. While slip-stick behavior has not been proven to have existed in the test discussed here, it would be consistent with the data.

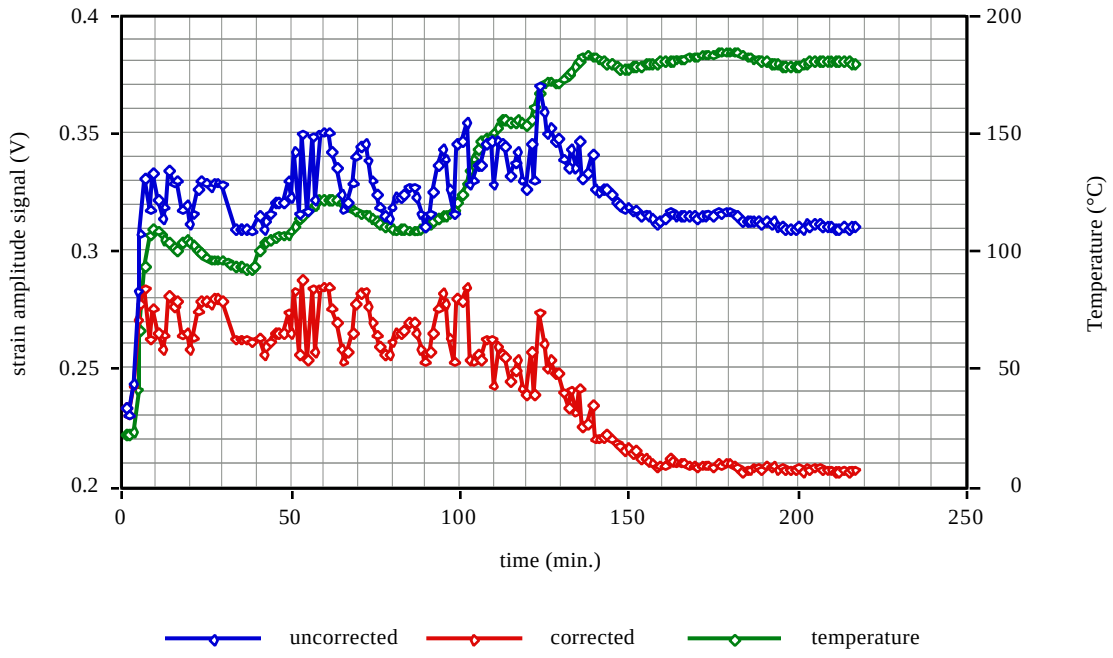

Figure 4-44. Temperature (green trace), strain amplitude signal output by lock-in amplifier (blue), and strain amplitude signal after subtraction of temperature effects (red).

By taking the tangent of the phase difference in Figure 4-43, and by applying Equation 33 to the strain amplitude signal of Figure 4-44, estimates for the absolute shear modulus and loss tangent are derived and displayed in Figure 4-45. An estimate of 10 μm was used for c in Equation 33, in keeping with the fiber spacing calculated in Appendix D. In the plot, the peak in loss tangent is coincident with a marked rise in the modulus, indicating the occurrence of gelation. No further transitions could be clearly discerned.

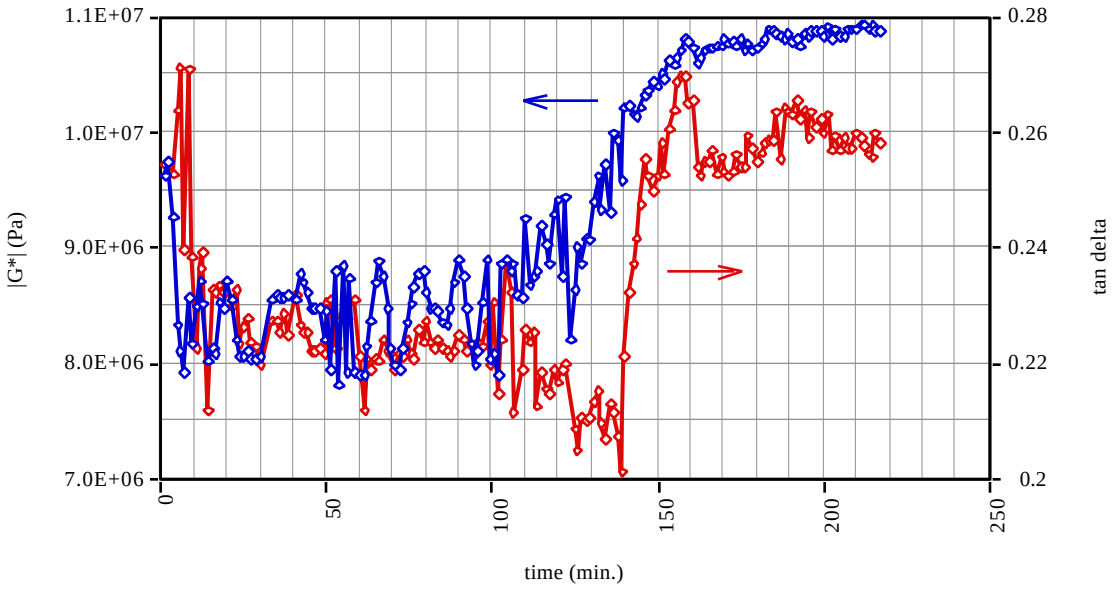

Figure 4-45. Output of sensor in Gr/EP prepreg after conversion of data to |G*| and tan delta (at 0.5 Hz).

Another sensor using a THUNDER® actuator was tested at Bell Helicopter Textron (Ft. Worth, TX) in a 32-ply Gl/Ep (glass fiber in a thermoplastic-toughened epoxy) prepreg cross-ply lay-up cured in a vacuum bag in an oven. The resin used in the Gl/Ep prepreg was identical to that used for the previous Gr/EP tests. The sensor survived the lay-up process, including pressing the sensor into the prepreg with a roller, followed by application of 15 psi consolidation pressure through a vacuum bag. A second sensor, employing a PZT (ceramic) actuator, did not survive the lay-up and consolidation process. The sensors were put in the laminate midplane, surrounded by two plies with 0° orientation (that is, parallel to the optical fiber leads) on both sides. In addition, three thermocouples (top, bottom, and midplane) and a dc conductivity sensor were added for logging by the data acquisition system. The dc conductivity sensor measured the ionic conductivity of the resin, which is proportional to the steady shear viscosity. A vacuum bag was added, and vacuum was applied. The lay-up was then cured under vacuum in the oven. The cure cycle for the prepreg used a 6 hour cycle, with a final soak at 176°C (350°F), and a couple of intermediate soaks at lower temperatures. Figure 4-46 shows the temperature profile used, as measured by a thermocouple in the oven.

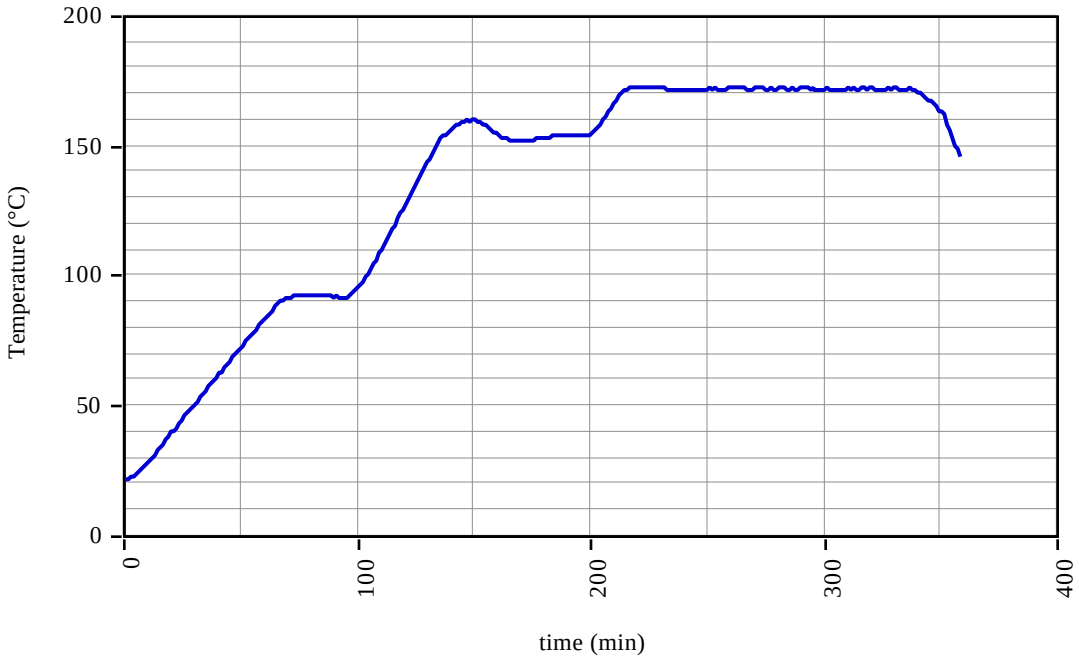

Figure 4-46. Temperature schedule used in test of sensor embedded in Gl/Ep prepreg.

The THUNDER®-based sensor continued to work throughout the cure cycle. As shown in Figure 4-47, the sensor strain amplitude increased at the beginning of the test, and leveled off at the first temperature soak (200°F). The strain amplitude dropped by about 90% over a period of approximately 15 minutes, starting at a time coincident with a dramatic rise in viscosity, as measured by the Bell conductivity sensor (in red in Figure 4-48). This drop in strain amplitude is consistent with the increase in absolute shear modulus expected during gelation. The relatively low strain levels measured, as compared to the tests in neat resin, are likely due to the close proximity of the reinforcing fibers to the actuator. As predicted by Equation 33, the strain magnitude output for a fixed resin shear modulus $|G^*|$ would be expected to be small for small values of the boundary separation c. The sensor had not been characterized for temperature dependence before the test; therefore, the variation of strain amplitude with temperature which is obvious at the beginning of the test could not be eliminated.

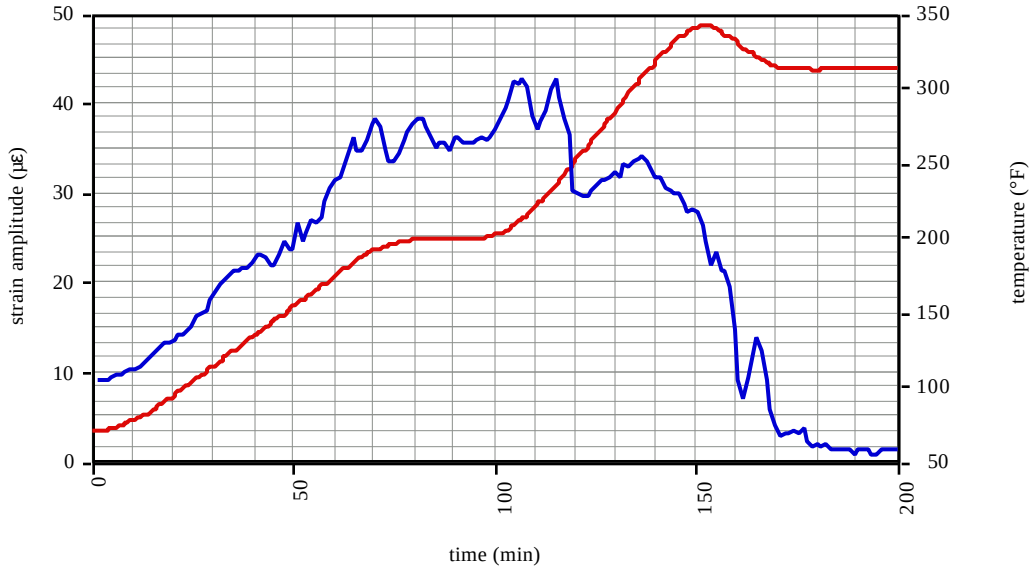

Figure 4-47. Temperature and strain amplitude for curing Gl/Ep prepreg.

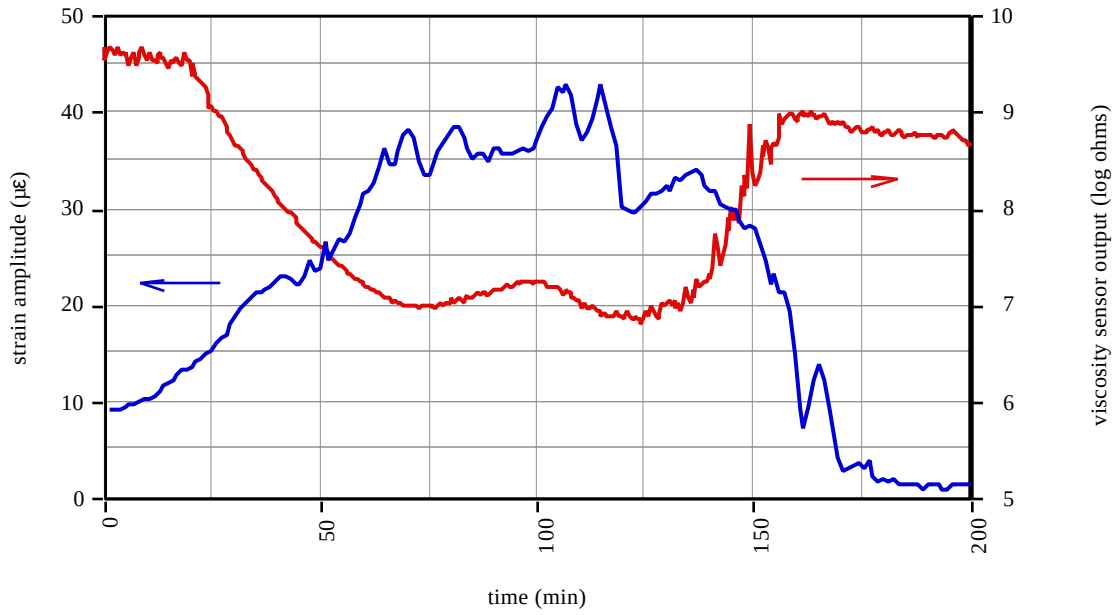

Figure 4-48. Strain amplitude output of sensor in curing Gl/Ep prepreg. Red curve is output of conductivity sensor (steady shear viscosity of resin is proportional to the resistance shown).

The strain amplitude data from
Figure 4-47 were converted to an estimate of the absolute shear modulus. As pointed out in Section 3.2, the output of the sensor when used in composite prepreg laminates is intended to be used for the monitoring of relative changes in the absolute shear modulus, due to the difficulty in exactly determining the boundary separation value *c*. For the estimate shown in Figure 4-49, a boundary separation value of 10 micrometers (10×10^{-6} m) was used. The results show that the modulus increases by more than an order of magnitude as the viscosity increases through gelation.

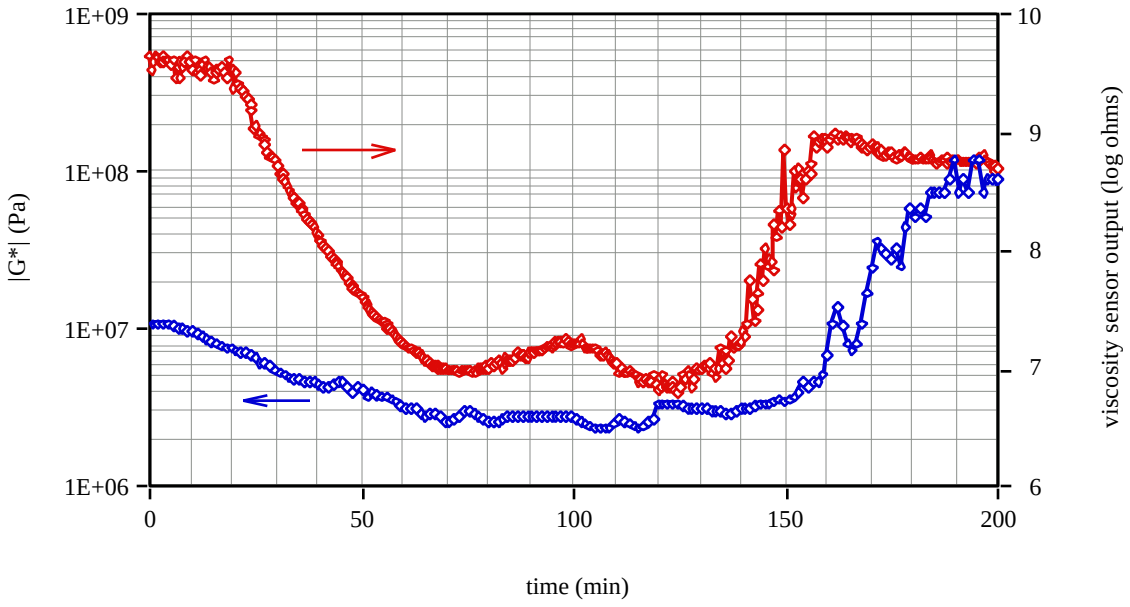

Figure 4-49. Plot of estimated absolute shear modulus for curing Gr/Ep epoxy, superimposed over output of viscosity sensor.

The loss tangent calculated from the phase output of the lock-in amplifier during the cure of the Gr/Ep is shown in Figure 4-42. No clear maxima that could be associated with gelation were detected, due to the poor signal strength resulting from the small strain amplitudes at the end of the test except with the possibility of the small peak seen immediately before data acquisition was terminated.

4.4 Temperature dependence of the PZT actuator

Changes in the temperature of a ceramic piezoelectric actuator cause a change in lattice spacing in the PZT crystal, resulting in a shift in the electrical impedance. This then causes a slight temperature dependent shift in the phase and amplitude of the actuator motion as a result of electrical excitation. To determine the magnitude of the impedance change, two wires were connected to the electrodes of a 5 mm x 15 mm x 0.18 mm PZT actuator with conductive epoxy. The actuator was suspended in an oven, and the wires were connected to the input of a Hewlett Packard HP4192A low frequency impedance analyzer. As the temperature of the oven was increased to 100° C, a laboratory computer acquired measurements of the impedance using a GPIB interface between the computer and the impedance analyzer over a range of frequencies from 5 Hz to 2 kHz. As the data for a frequency of 10 Hz demonstrates in Figure 4-51, the real part of the impedance exhibits a slight increase in value with increasing temperature. The reactive impedance is negative, implying that the impedance is largely capacitive, and increases more dramatically with temperature.

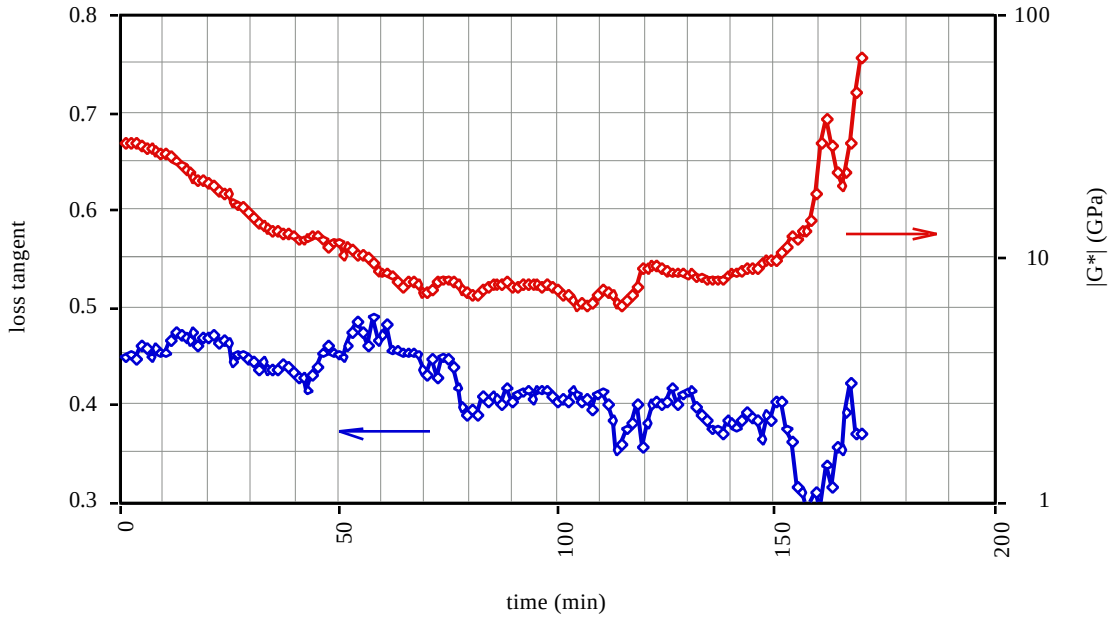

Figure 4-50. Tan delta output of sensor in curing Gl/Ep prepreg. Data acquisition past 170 minutes was terminated, as the signal was too noisy to determine tan delta reliably (due to decrease in strain amplitude signal, as shown in Figure 4-39 above).

Figure 4-47 shows linear fits to the data, with the associated equations for the lines. The use of a linear fit to extrapolate the temperature dependence over a limited extension of temperature beyond the measured data was justified by Krishnamurthy.[44] Due to difficulties in deriving themoelectomechanical constitutive models of temperature effects in piezoelectric materials, the author relied upon empirical tests to show that the impedance of PZT-5A varies linearly with temperature over a limited temperature range.

In principle, it should be possible to predict the change in signal amplitude and phase resulting from temperature changes from the linear fits to the data in Figure 4-47. However, that has not yet been attempted during the course of this research.

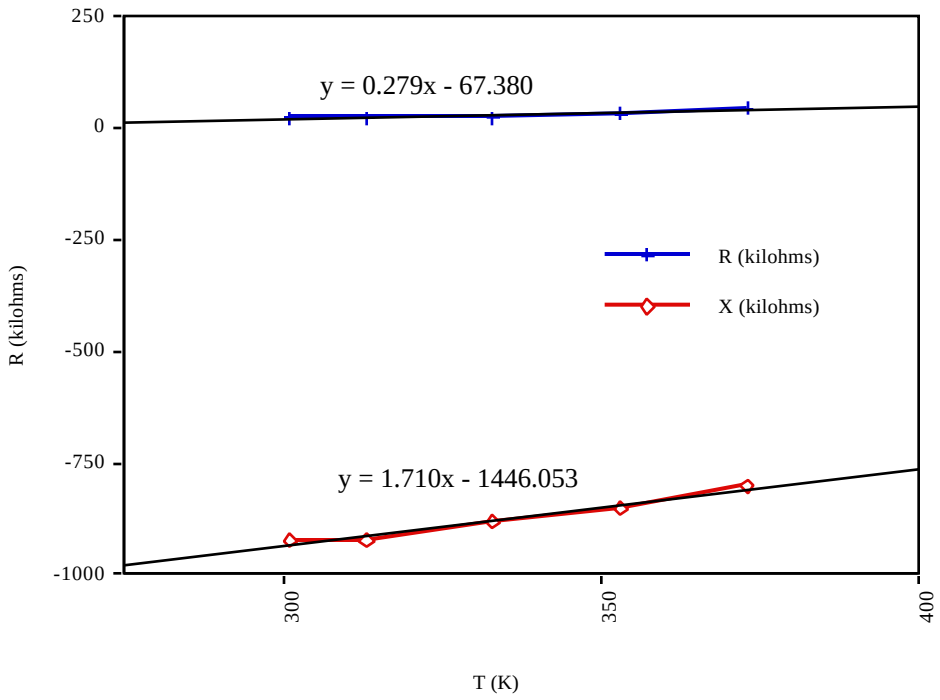

Figure 4-51. Temperature dependence of the electrical impedance of the PZT piezoelectric actuator.

4.5 Miniaturization of sensors

While the prototype sensors described above have proven useful in demonstrating the feasibility of the miniature dynamic mechanical analysis approach to cure monitoring, those sensors are not practical for embedded measurements in composite laminates. With a surface area of about 50 square millimeters, one of the prototype sensors would generate inclusions that might lead to delaminations in the composite. Consequently, some of the effort of this research has been directed towards miniaturization of the sensor in order to permit it to be embedded without deleterious effects to the composite strength.

The most straightforward approach towards sensor miniaturization would be to integrate the actuator directly into the EFPI fiber optic strain gage. Two methods that were investigated were the coating of the glass capillary alignment tube with an active material such as a piezoelectric or magnetostrictive material, and the replacement of the glass tube entirely with a tube made entirely from such an active material.

As a first step in this direction, a one centimeter long glass tube with an outside diameter of 360 μm and inside diameter of 130 μm was sputter coated with a thin film of Metglas®, a magnetostrictive amorphous metal alloy of boron and silicon manufactured by Allied Signal, Inc. In addition, two planar borosilicate glass microscope slides were also coated with Metglas for later analysis of the coatings. A magnetostrictive material was chosen for the first investigation of actuator coatings because they are easily sputtered and can be activated magnetically without the need to attach wires or electrodes to the actuator. A Denton vacuum evaporation system was modified by adding a single planar magnetron cathode for dc magnetron sputtering, and a rotary mechanical coupler was added to the bell jar to allow the fiber to be rotated during the thin-film deposition. The sputtering target was prepared by adhering Metglas® foil to a copper substrate. Attempts to use a 25 mm diameter by 1.6 mm thick Metglas® disk as a target were less successful, because the high permeability of the Metglas® target, which is ferromagnetic, tends to confine the magnetic flux lines in the magnetron sputtering head, reducing the sputtering rate. Confinement of magnetic flux lines is reduced by the use of a thin Metglas® foil as target. The fiber used was a homogeneous 400 μm diameter glass fiber, drawn from GE-214 fused quartz stock on the Virginia Tech fiber draw tower. With the fiber positioned approximately 40 mm from the target, a coating of approximately 1.5 μm thickness was produced by sputtering for 33 minutes. Cross-sectional scanning electron micrographs of the fiber indicated that the coating had a columnar structure.

Samples of the coating were examined using X-ray diffraction (XRD) analysis, to determine if the coating was amorphous. An amorphous coating, which is required for proper

magnetostriction in the material, was expected due to the low temperature used for the sputtering process. Under such conditions, the deposited material is quenched before it reorganizes into a crystalline structure. The XRD tests showed no crystallinity in the as-sputtered coatings. One sample of the sputtered coating was annealed at 520°C, in excess of the 507°C crystallization temperature of Metglas®. XRD analysis on this sample detected crystallization, lending further weight to the conclusion that the coatings that were not annealed were in fact amorphous.

To test the magnetostriction of the coatings, a fiber optic extrinsic Fabry-Perot interferometer (EFPI) sensor, configured as an extensometer, was attached to the surface of one of the coated glass rods. As a control, a second EFPI sensor was attached to the surface of a commercially obtained Metglas® foil substrate. The assemblies were then placed in a solenoid, and a dc current was applied to the solenoid. A distinct change in the length of Metglas® foil was measured upon application of the dc current, but no changes were observed in the length of the coated glass rod.

An analytical prediction of the expected mechanical strains in the coated glass tube due to magnetostriction of the coating was undertaken, to gain some insight into the causes for the lack of observed actuation. According to data supplied by Allied Signal, the saturation magnetostriction is 30 microstrain. Since the elastic modulus of the Metglas® foil is approximately 100 GPa, this implies that the maximum magnetostrictively generated stress is

$$\sigma_{\max} = E\,\varepsilon_{\max} = \left(100x10^{9}\frac{N}{m^{2}}\right)\left(30x10^{-6}\right) = 3\,x10^{6}Pa. \tag{74}$$

For a Metglas® thin film of 1.5 μm thickness on a cylinder of 130 μm diameter, the maximum force that could then be generated by the film would be

$$F_{\max} = \sigma_{\max}\,A = \left(3x10^{6}\frac{N}{m^{2}}\right)\left(\pi 130x_{10}{}^{-6}m\right)\left(1.5x_{10}{}^{-6}m\right) = 1.84x10^{-3}N. \tag{75}$$

Assuming perfect traction between the Metglas® coating and the glass tube so that the force is the same in both, the stress generated in the glass tube is

$$\sigma_{glass} = \frac{F}{A_{glass}} = \frac{1.84x10^{-3}\,N}{\left[\pi\left(\frac{320\mu m + 130\mu m}{2}\right)\right]\left(\frac{320\mu m - 130\mu m}{2}\right)} = 2.7x10^{4}Pa. \quad (76)$$

where the inner diameter of the tube is 130 μm. Since the elastic modulus of fused silica glass is 72 GPa, the maximum resulting strain that would be expected to be observed in a glass tube with a 1.5 μm thick Metglas® coating is

$$\varepsilon_{glass} = \frac{\sigma_{glass}}{E_{glass}} = \frac{2.7x10^{4}Pa}{72x10^{9}Pa} = 3.7x10^{-7} = 0.37\ \mu\varepsilon. \quad (77)$$

Since the minimum change in strain that can be resolved by the strain gage signal processing system used to interrogate the EFPI strain gage is about one microstrain ($1x10^{-6}$), the largest strain that could be expected to develop in the Metglas® coated strain gage would not be observable. This very small resulting strain is likely the reason that no magnetostriction was observed in the test of the coated tube during magnetic actuation.

A similar analysis can be used to show that the maximum strain that could be generated by a one micrometer thick film of PZT on a one centimeter long glass tube with 320 μm OD and 130 μm ID is on the order of 0.01 microstrain, well below the minimum resolvable strain change with the instrumentation used for this research. For this reason, further effort was directed toward the second alternative to sensor miniaturization, specifically the fabrication of piezoelectric microtubes. Since it is the high modulus or stiffness of the glass tube in Equation 77 that is in large part responsible for the small strains developed, then it should be possible to develop sufficient strain to result in observable motion of the strain gage by replacing the glass tube entirely with a piezoelectric tube. A sensor with a design similar to the one depicted in Figure 4-52 was contemplated.

Previous reported attempts to fabricate piezoelectric microtubes have been less than optimal. Fox, et. al, produced PZT microtubes by sputter depositing a platinum electrode on a sacrificial polyester fiber.[44] A layer of PZT a few micrometers thick was then deposited by DC magnetron sputtering, followed by deposition of an outer platinum electrode.

---

[44] Glen R. Fox, Claude A.P. Muller, Matthius Kuhn, Nava Setter, Nguyen Hong Ky, Hans Georg Limberger, "Piezoelectric fiber optic modulators and micro-tubes," SPIE Vol. 2641, *Microelectronic Structures and Microelectromechanical Devices for Optical Processing and Multimedia Applications*, Oct. 1995, pp. 55 - 61.

Annealing was used to crystallize the deposited PZT layer, while pyrolyzing the polyester fiber, leaving a hollow tube. The tubes achieved in this manner demonstrated a large amount of porosity, which was attributed by the authors to evaporation and outgassing of lead oxide (PbO) from the active layer .

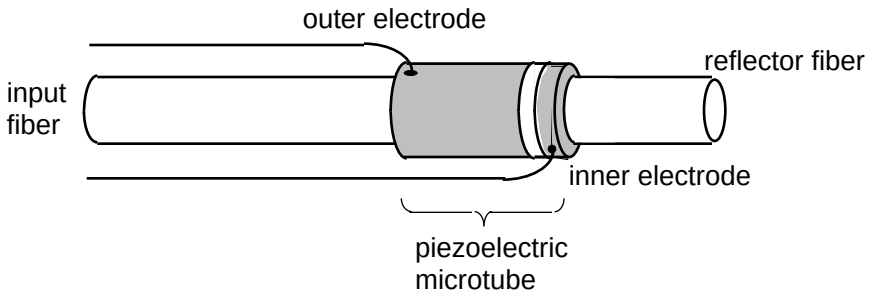

Figure 4-52. Miniature rheometer sensor employing piezoelectric microtube for actuation.

To develop a suitable piezoelectric microtube, CeraNova, Inc. of Boston, MA, was contracted.[45] To produce the required tubing, CeraNova proposed extruding a PZT-5A slurry (a suspension of PZT powder in propanol) onto a polyester fiber, by drawing the fiber through a bath of the slurry, followed by a die, as depicted in Figure 4-53. After extrusion, the coated fiber is heated in an oven at a temperature sufficiently high to evaporate the propanol solvent. Following this step, the fiber and coating are heated at a high temperature to pyrolyze the polyester fiber, while simultaneously sintering the PZT into a dense ceramic. The result should be a PZT microtube which will demonstrate piezoelectric properties after poling.

Initial attempts by CeraNova to manufacture the tubes resulted in tubes that had poor concentricity of the inner bore with the outside diameter of the tube, leading to thin walls and perforations in places. The cause for the lack of bore concentricity appeared to be due to difficulty in aligning the polyester fiber in the center of the die during the extrusion process. As Figure 4-53 illustrates, if the polyester fiber drags along one side of the die during extrusion, the resulting tube will have a thin wall.

[45] CeraNova Corporation, 101 Constitutional Blvd. Suite D, Franklin, MA 02038.

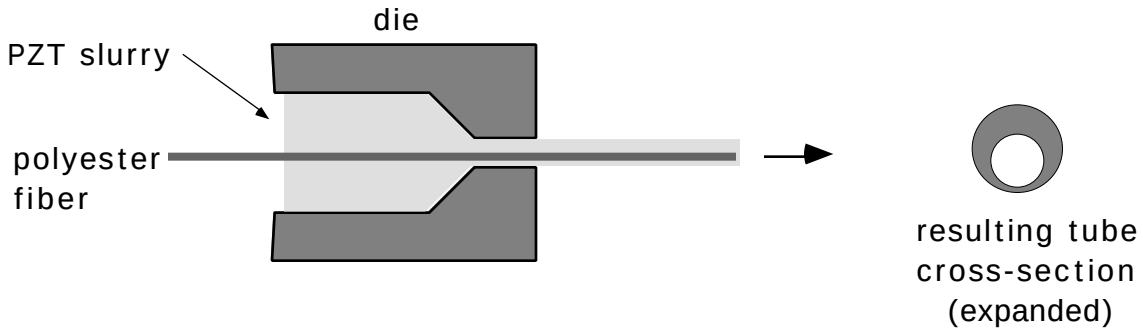

Figure 4-53. Schematic showing extrusion of PZT slurry onto polyester fiber.

To improve the wall concentricity, it was decided to use the coating extrusion system on the Virginia Tech fiber draw tower to coat PZT onto the polyester fiber. An apparatus was set up to provide payout of the fiber through a coating cup with an interchangeable die. In Figure 4-54a, the polyester fiber is paid out from the spool at the top of the figure. After passing through a coating cup (Figure 4-54b) which contained the PZT slurry, the fiber exited the cup through a precision die which defined the outside diameter of the coating. A heat gun under the coating cup was used to drive off the propanol solvent, before the fiber entered the capstan wheel. The capstan was used to pull the fiber at a constant rate through the cup. As the fiber exited the capstan, it was wound onto a spoon, seen in the bottom of Figure 4-54a.

Through trial-and-error, it was determined that the most uniform coating was produced by drawing the coated fiber several times through the slurry, using a succession of progressively larger dies. Eleven coatings of PZT were applied to seven meters of 200 μm (0.008 in) diameter polyester fiber using the dies listed in Table 1. The final coating diameter was 370 μm (0.0146 in). The spool of seven meters of coated fiber was shipped to CeraNova, which processed the fiber by pyrolyzing the polyester fibers and sintering the PZT. The resulting tubes were measured to have outside diameters of 270 μm (0.011 in) and inner diameters of 140 μm (0.0055 in), making them well suited for assembly of EFPI strain gages.

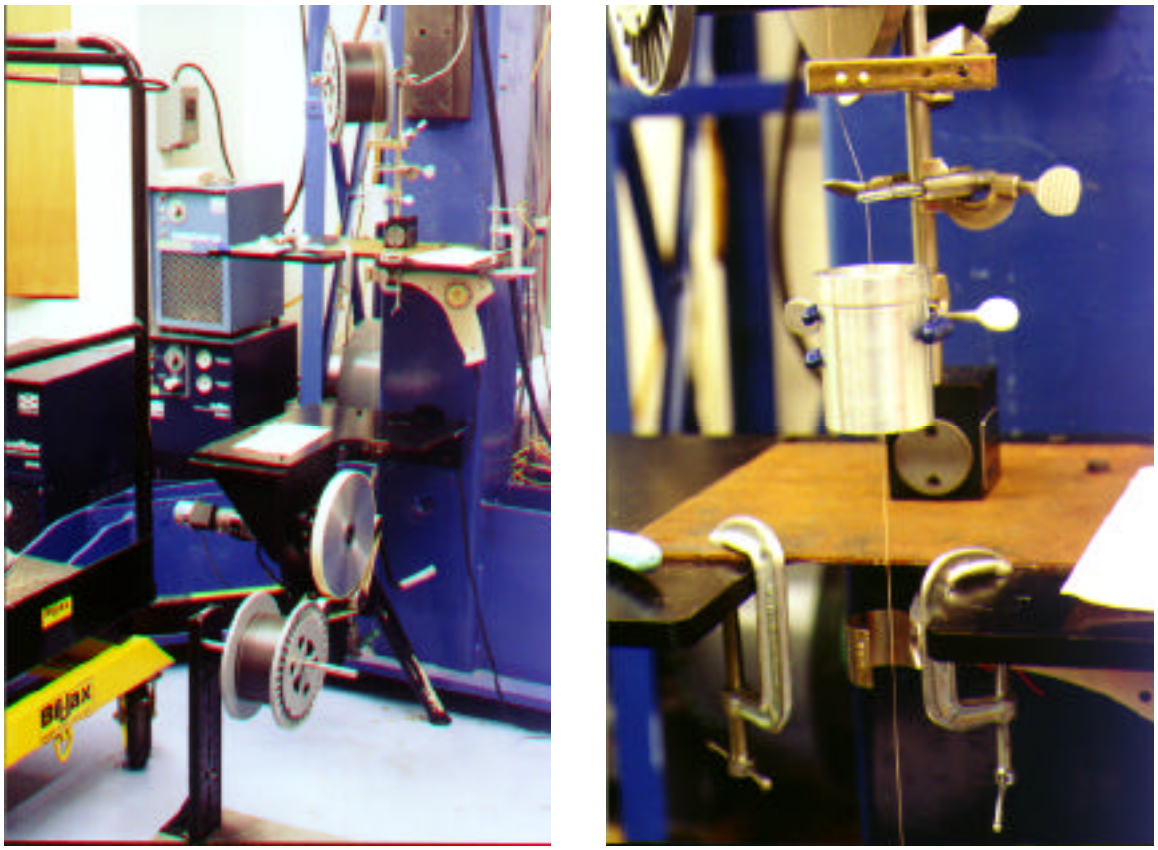

Figure 4-54

a. Apparatus used to coat polyester fiber with PZT slurry.

b. Close-up of coating cup, showing fiber passing through cup.

Table 1. Die diameters used for coating PZT onto polyester fiber.

Die diameter (μm, in)	Number of coats
216, 0.0085	two
284, 0.0122	three
320, 0.0126	three
381, 0.0150	three

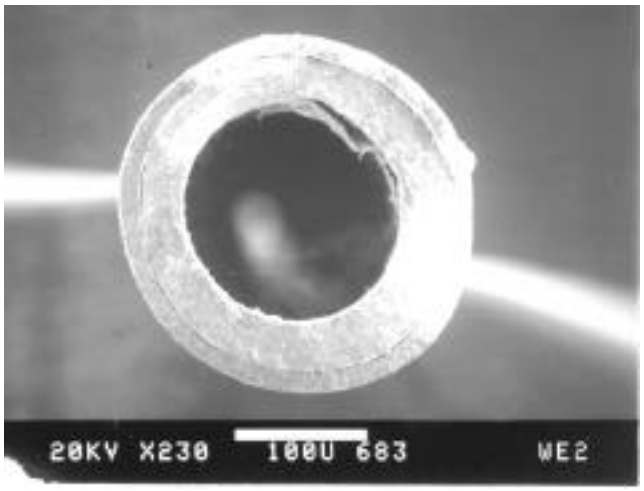

Figure 4-55. Scanning electron micrograph on cross-section of PZT microtube after sintering.

In order to use the PZT tubes as piezoelectric devices, they require poling to produce a remnant polarization of the crystalline structure. Poling of PZT-5A ceramics requires the application of a 10 - 20 kV/cm electric field at a temperature of 80 - 100°C for at least 20 minutes. In order to apply the electric field across the wall thickness of a tube, it is necessary to coat the outside surface and the inner wall of the tube. Coating of the outer surface of the tube may be accomplished relatively easily by physical deposition, such as sputtering or evaporation. However, due to the small dimensions of the inner bore of the tube, physical deposition cannot be used for creation of the inner electrode.

The most promising approach to the deposition of metallic thin films to the inner wall appears to be electroless plating of copper or nickel. This process, which utilizes catalytic reduction of the metal ions on the surface of the substrate to be coated, produces dense, nonporous, amorphous coatings. Initial experiments directed towards electroless copper coating of the PZT microtubes were unsuccessful, as the plating solution would not fill the tubes by capillary action. The use of a pump to fill the tube interior is suggested in Chapter 6.

4.6 Micromachined housing for viscoelasticity sensor

For applications where it is desired to determine the value of the storage or loss moduli, it will be necessary to fix the actuator-boundary separation to a known and unchanging value. Section 4.1 describes one approach to accomplishing this, wherein a housing of fixed dimensions is assembled around the actuator-strain gage assembly. In order to explore the feasibility of this approach, several sensors were fabricated with housings made from micromachined silicon parts. Silicon micromachining was chosen for production of the housing, due to the need for close control of the dimensional tolerances of the parts. Since small sizes are required for the housing components, tight tolerances will be required in order that variations in the actuator-boundary separation not contribute to errors in the determination of the moduli. In the rapidly emerging field of micromachining, techniques from semiconductor manufacturing are used to fabricate microscopic mechanical assemblies in silicon substrates. In the most widely practiced approach, photolithography is used to mask off regions of a silicon wafer, and then those unmasked regions are etched away using anisotropic etchants. Miniature vibrating beams, rotating gears, and even microscopic motors have been made in this way. Since hundreds of sensors may be micromachined simultaneously, in the same way that hundreds of integrated circuits are made from a single silicon wafer, the economy of scale will result in low costs per sensor. And because the features of the mechanical assembly are defined with tolerances on the order of microns, the geometry will be reproducible, resulting in a sensor that is accurate and repeatable.

The initial design for the micromachined housing is shown in Figures 4.1 and 4.2. As they illustrate, two pieces labeled as spacers clamp one end of the actuator, and suspend two flat plates above the actuator, one on each side. The spacer has a slot for ingress of the optical fiber and the actuator wires, and is designed so that two identical spacers are mated to clamp the actuator. Similarly, the top and bottom plates are identical, to simplify construction of the housing and reduce manufacturing costs. The sides of the housing were left open, to facilitate flow of the viscous resin into the cavity containing the actuator. In practice, however, it was found necessary to include posts to connect the two free ends of the plates, to keep the plates from vibrating, and to ensure that the actuator-boundary separation was constant. In addition, three small holes were included in the plates to permit air to escape when the sensor housing is immersed in the test fluid.

Litton Poly-Scientific of Blacksburg, VA was contracted to produce the micromachined silicon elements. Four-inch diameter, 100-oriented silicon wafers were used, permitting 40 plates to be produced with each wafer. The thickness of the wafer used to produce the parts used to assemble the housings tested was 0.500 mm. The etch angles for the three holes in the plates and for the slots in the spacers was 54° with respect to the horizontal (the plane of

the wafer). Since the plates and spacers were diced from the wafer, the sides of those parts were perpendicular with respect to the horizontal.

A photograph of one of the completed devices is shown in Figure 4-56. The electrical wires, with red polyurethane insulation, emerges from the spacers at the rear of the unit. The optical fiber lead also passes through the same port in the spacers, but is difficult to see in the photograph. One of the posts used to support the free end of the plates can be seen at the near corner of the device.

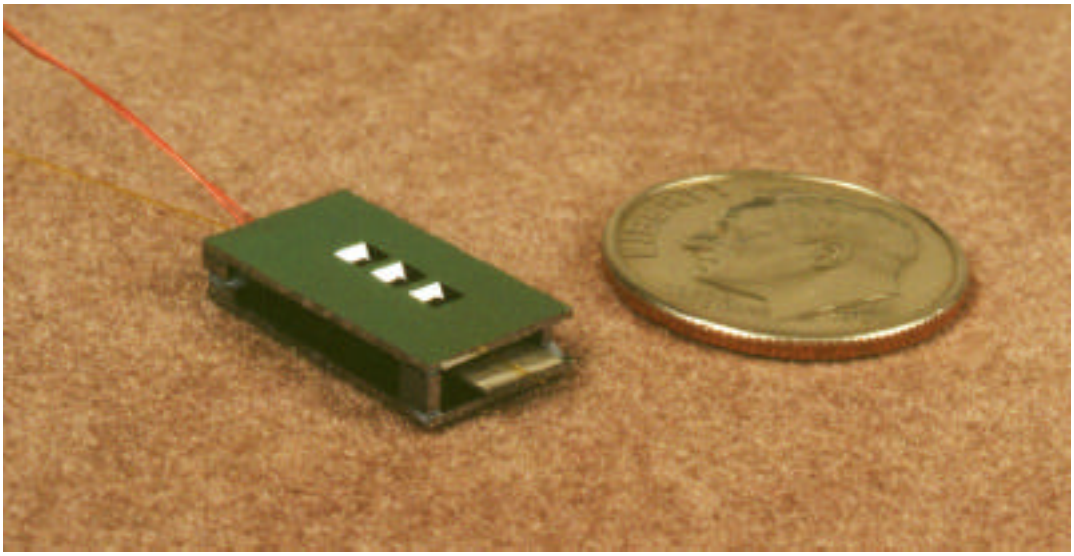

Figure 4-56. Viscoelasticity sensor with micromachined silicon housing, next to a dime for a comparison of size.

One of the sensors with integral housing was tested in curing RTM-1 epoxy. First, the temperature dependence of the sensor was evaluated, by suspending the sensor inside and oven, and recording the outputs as the temperature was varied. The results in Figure 4-57 and Figure 4-58 reveal a definite sensitivity to temperature changes. By fitting the data to a linear model, the phase sensitivity was found to be 1.5×10^{-2} °C^{-1}, while the strain amplitude sensitivity was calculated to be 0.25% °C^{-1}.

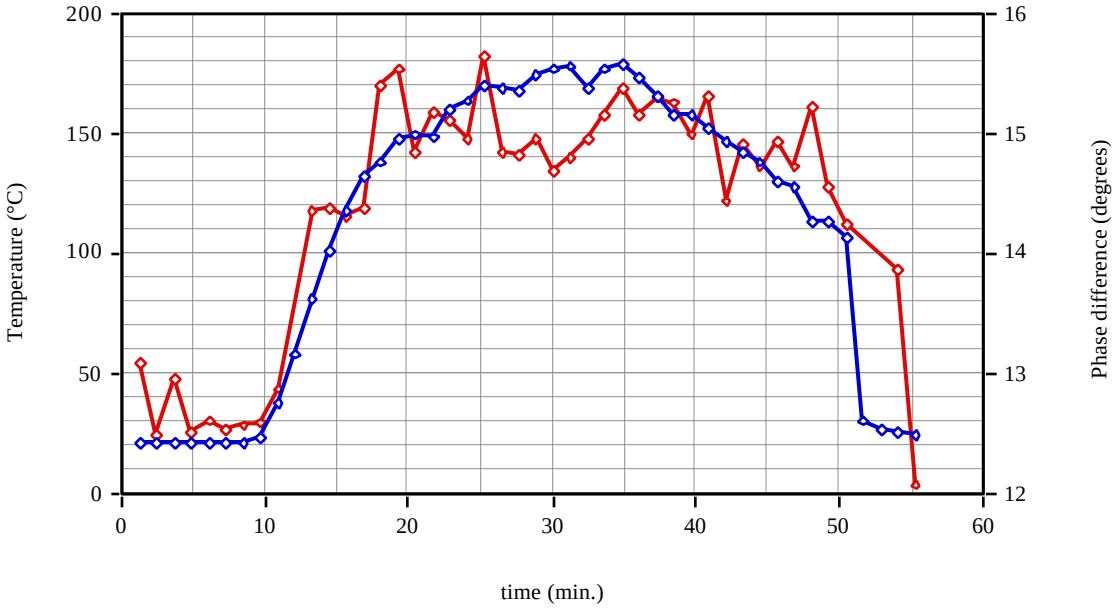

Figure 4-57. Variation of phase output of sensor and micromachined housing with temperature.

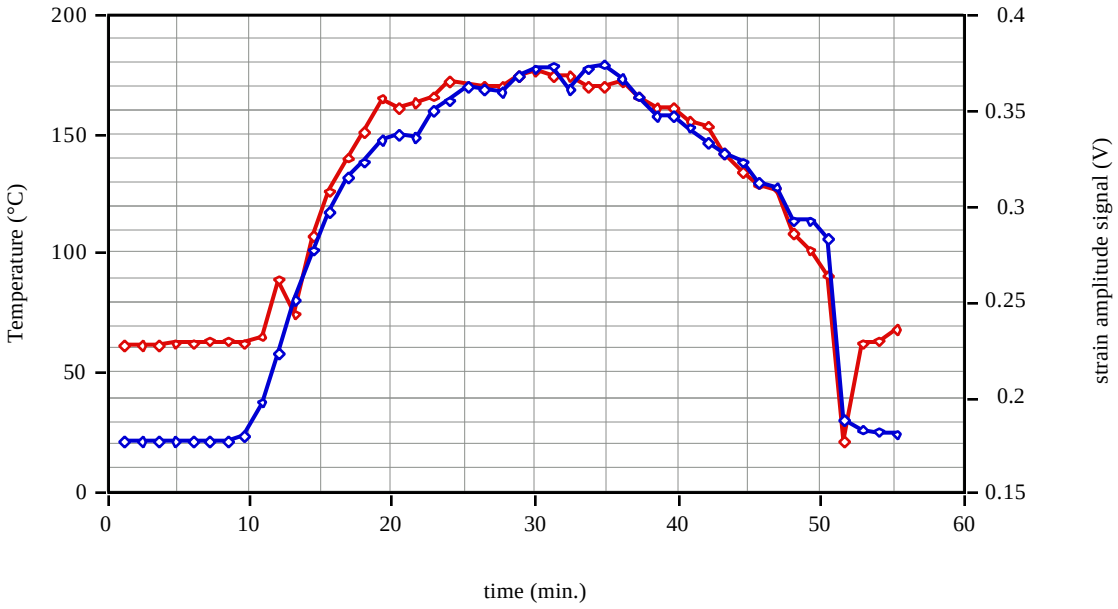

Figure 4-58. Variation of strain amplitude signal of sensor and micromachined housing with temperature.

The sensor was placed in a 2 in diameter aluminum dish, which was then heated to 90°C in an oven, while a sample of RTM-1 resin was heated to 90°C, to reduce its viscosity and permit pouring. After sufficient resin was poured into the dish to cover the sensor and housing, the data acquisition was started and the temperature was increased to 180°C.

The output obtained in Figure 4-59 suggests that little temperature correction was required for the phase output. Figure 4-60 shows a greater degree of temperature sensitivity in the strain amplitude. Since the temperature of the oven used to heat the sample was set manually, some oscillations in the temperature is observed as the final temperature setpoint was overshot and corrected. The oscillations are reproduced in the strain amplitude output of the sensor in Figure 4-60. After correction of the data to remove the temperature dependence, the oscillations were greatly reduced. What remains is a gradual decrease in the strain amplitude due to the increasing elasticity of the epoxy.

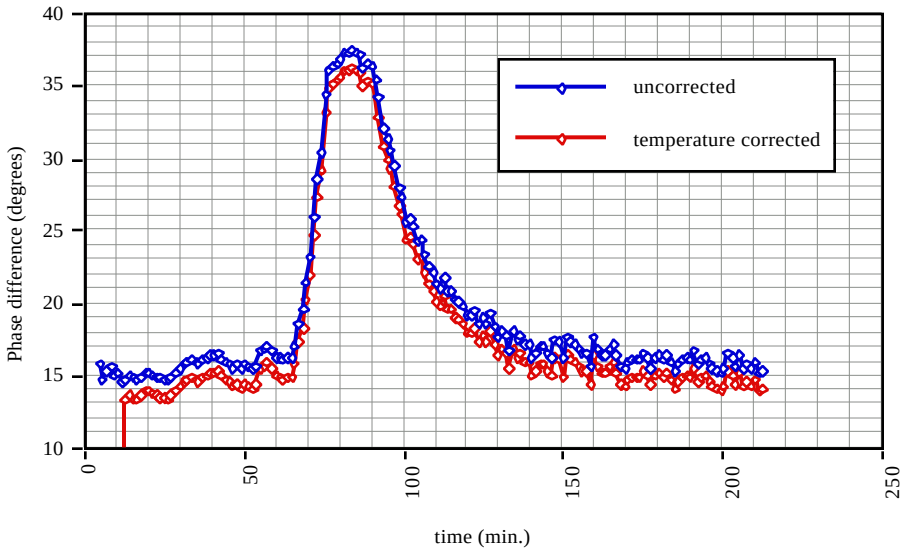

Figure 4-59. Phase difference output of sensor and micromachined housing before and after correction for temperature effects.

By the application of Equation 33, an estimate for the absolute shear modulus of the epoxy as a function of cure time is determined and plotted in Figure 4-61. Using a value of 0.825 mm for *c*, which was determined through the use of direct measurement with a micrometer, a final value of approximately 9 GPa. This calculated value is somewhat higher than the value of 5.7 Gpa obtained during characterization of the RTM-1 by the Netzsch DMA (Figure 4-24).

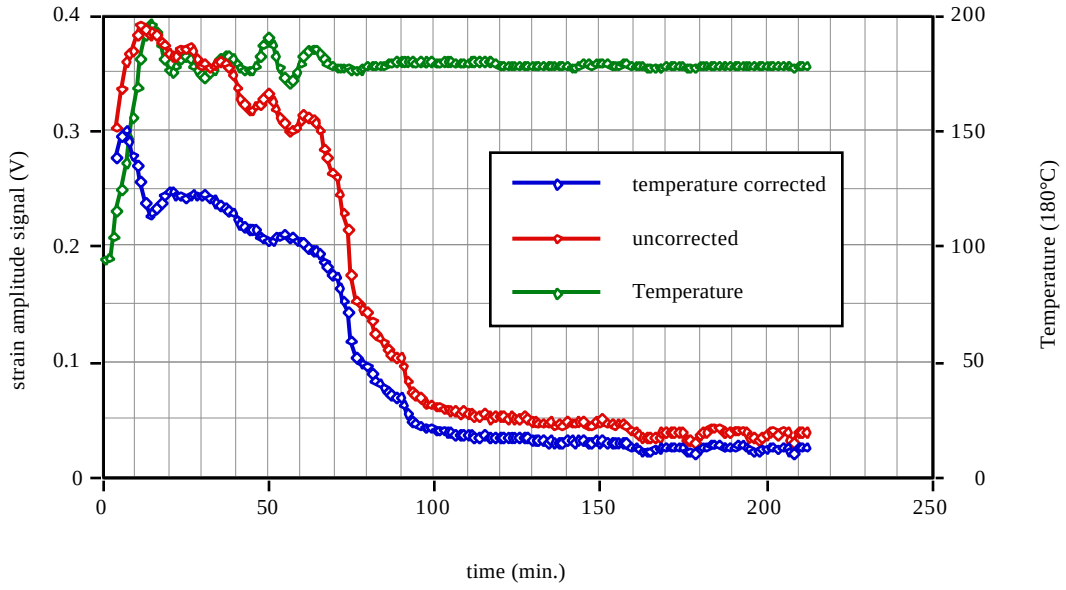

Figure 4-60. Strain amplitude signal of sensor and micromachined housing before and after correction for temperature effects.

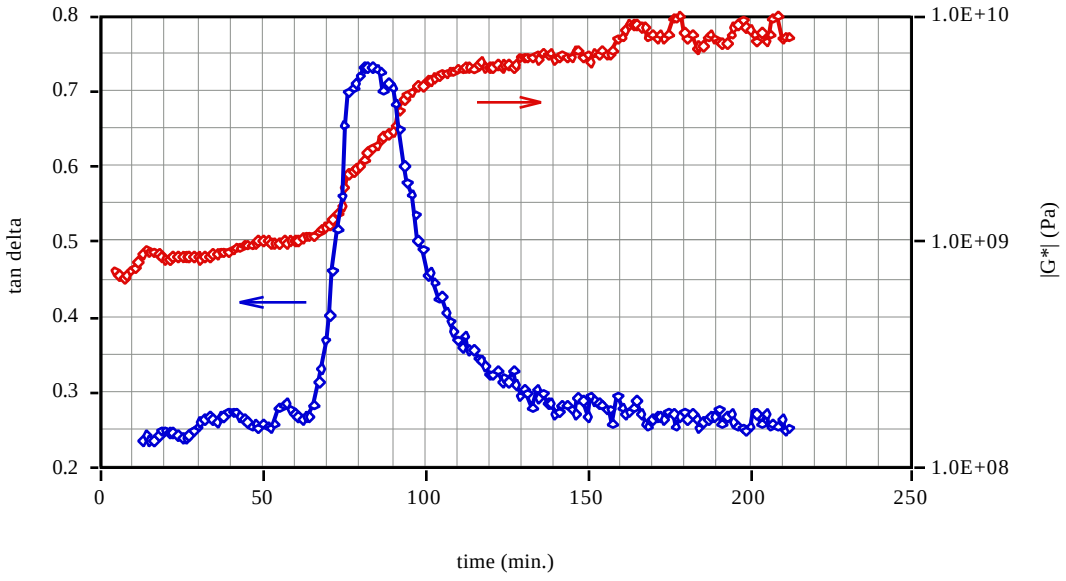

Figure 4-61. Loss tangent and absolute shear modulus of RTM-1 epoxy cured at 180°C, as measured by sensor with micromachined housing.